FSLAM: A QGIS plugin for fast regional susceptibility assessment of rainfall-induced landslides

Zizheng Guo[1, 2]*, Ona Torra[1], Marcel Hürlimann[1], Clàudia Abancó[3], Vicente Medina[1]

[1] *Division of Geotechnical Engineering and Geosciences; Department of Civil and Environmental Engineering, UPC BarcelonaTECH; 08034 Barcelona, Spain*

[2] *School of Civil and Transportation Engineering, Hebei University of Technology; 300401 Tianjin, China*

[3] *Department of Mineralogy, Petrology and Applied Geology, Faculty of Earth Sciences, University of Barcelona; 08028 Barcelona, Spain*

* Corresponding author: Zizheng Guo (cuggzz@cug.edu.cn)

Abstract: Shallow slope failures triggered by rainfall commonly pose considerable risks in mountainous areas. In order to delineate areas where landslides are more prone to occur within a region, we have designed and developed a Python QGIS plugin named Fast Shallow Landslide Assessment Model (FSLAM). The plugin integrates a simplified hydrological model and a geotechnical model based on the infinite slope theory and contains two principal modules: runoff and slope stability modelling. It can output up to 15 raster maps describing the hydrological and stability conditions in a short computational time. Firstly, we explain the design of graphical user interface and the elements of the plugin. Then, the Berguedà area in NE Spain is used as case study to present the procedure of the plugin application. The results show that the accuracy of landslide susceptibility assessment performed by FSLAM-plugin is high and the computing time is only a few minutes.

Keywords: Landslide susceptibility; Python; QGIS plugin; Rainfall; Runoff

1. Introduction

Shallow landslides induced by heavy rainfall are a global issue, which are posing severe implications for mountain environments (Baum and Godt, 2010; Froude and Petley, 2018). For scientists and stakeholders dealing with shallow slope failures, accurate landslide susceptibility maps at regional scale are necessary information. They can identify the areas that are spatially prone to landslides (Guzzetti et al., 2005). Hence, landslide susceptibility assessment is considered as a key tool for the understanding of the spatial distribution of landslides and can help decision makers on the design of landslide risk reduction strategy (Guzzetti et al., 1999; Fell et al., 2008).

Landslide susceptibility models can roughly be divided into heuristic models, physically-based models, statistical models and machine learning models (Fell et al., 2008; Zêzere et al., 2017; Broeckx et al., 2018; Reichenbach et al., 2018; Merghadi et al., 2020). Among them, physically-based models incorporate soil properties into the susceptibility analysis, as they are normally based on geotechnical slope stability equations driven by hydrologic inputs (Wang et al., 2019). On the contrary, the other models are typically independent from the physical processes of landslides initiation and runout (Strauch et al., 2019). Physically-based models therefore, have advantages in helping to understand the mechanisms of slope failures, especially regarding the effects of rainfall.

Although physically-based models for landslide susceptibility assessment are popular (e.g., Montgomery and Dietrich, 1994a; Rigon et al., 2006; Baum et al., 2008; Lehmann and Or, 2012; Mergili et al., 2014), each of them has its particular drawbacks, which can be grouped in two main groups: (i) Large uncertainty associated with soil properties. It may strongly influence the model performance due to the inherent variability of input parameters (Tofani et al., 2017). (ii) High computational cost. As a result of the incorporation of a comprehensive approach for the rainfall infiltration in unsaturated soil (Iverson, 2000), model calculations can last from several hours to even several days (e.g., Rossi et al., 2013). To overcome these limitations, an open-source code named Fast Shallow Landslide Assessment Model (FSLAM) has been proposed (Medina et al., 2021). It does not only allow using soil properties as stochastic parameters, but it can also obtain landslide susceptibility maps of large regions within a few minutes. However, the FSLAM code was initially not implemented into a plugin and did not have a Graphical User Interface (GUI), which made it difficult to use.

Plugins are an essential component of software, which can extend the capabilities of an already existing software as well as improve the user experience by providing more user friendly GUI, without affecting the source code (Sela et al., 2019). Plugins are available for many commonly used web software, such as web browsers (Google Chrome, 2018), free and commercial engineering software, like AutoCAD (AutoDeskInc, 2015), Quantum GIS (QGIS, QGIS Development Team, 2021), as well as for word processors and video editing software. Although plugins are not required for the use of the original application, third-party users are highly encouraged to develop new features, which can reduce the burden of the main developers.

Within the framework above, many plugins have been developed, especially the ones for geosciences modelling based on QGIS platform (Nielsen et al., 2017; Criollo et al., 2019; Ellsäßer et al., 2020). Among them, some plugins can be used for natural hazards spatial analysis and modelling, such as QVAST (QGIS for VolcAnic Susceptibility, Bartolini et al., 2013), Susceptibility Zoning plugin (Titti and Sarretta, 2020) and LaGriSU (Landslide Grid and Slope Units, Althuwaynee, 2021). However, these plugins are mainly used for pre-processing of landslide mapping (e.g., LaGriSU is used for landslide samples extraction in QGIS) or apply statistically-based methods to perform landslide susceptibility mapping (e.g., the Susceptibility Zoning plugin applies the frequency ratio and weight of evidence methods). A plugin based on physical model for regional landslide susceptibility assessment is not available so far. Hence, to contribute to filling this gap, we developed a Python QGIS plugin for the newest version of the FSLAM code.

The main objectives of the present work are: (i) presenting and describing in detail a plugin developed in PyQGIS based on the FSLAM code (Medina et al., 2021); (ii) showing and describing all the outputs associated with the newest version of FSLAM, including 15 raster maps and 6 text files, (iii) applying the FSLAM-plugin to the study area Berguedà (Spain) to assess the landslide susceptibility and present the whole application of the plugin in a scientific context.

2. Methods

2.1. FSLAM model description

There are two main parts included in the FSLAM model: One is the stability modelling, where slope stability is computed using two hydrological approaches and the infinite slope theory. The other one is the runoff modelling, which calculates the peak water discharge in each cell of the study area. The main aspects of both of them are explained in the sections below, while further details on the previous version of the stability calculation can be found in Medina et al (2021).

2.1.1. Stability modelling

The stability modelling includes two different sub-models, namely the geotechnical model and the hydrological model (Medina et al., 2021). The former employs the infinite slope theory to calculate the slope stability (Lambe and Whitman, 1979; Pack et al., 1998), where the factor of safety (*FS*) can be computed by:

$$FS = \frac{C_r + C_s}{g\rho_s z \cos\theta \sin\theta} + \left(1 - \left(\frac{h}{z}\right)\left(\frac{\rho_w}{\rho_s}\right)\right)\left(\frac{\tan\varphi}{\tan\theta}\right) \quad (1)$$

where C_r (kPa) is the root cohesion from the vegetation, C_s (kPa) is the effective cohesion of soil, g (m/s^2) is the gravity, ρ_s (kg/m^3) is the density of the saturated soil, z (m) is the soil depth, h (m) is the position of the water table, θ (°) is the terrain slope, ρ_w (kg/m^3) is the density of water, φ (°) is internal friction angle.

In the next step, the hydrological model is used to compute the rainfall infiltration into the soil layer and the position of the water table. The FSLAM model integrates lateral flow and vertical flow to achieve this task: First, the lateral flow method is used to determine the increase of the water table (h_a, (unit: m)) related to the effective antecedent water recharge (q_a, (unit: mm/d)), associated to the rainfall occurred in the period preceding the landslides. The q_a is defined as a reduced percentage of the precipitation due to the runoff and evapotranspiration, and can also be considered as the effective water infiltration into the soil layer (Medina et al., 2021). It provides the initial condition for landsliding. It should be noted that in Medina et al. (2021), the antecedent water recharge was called antecedent rainfall (P_a, (unit: mm)). However, this term was confusing and thus we renamed it both in the present paper and the QGIS plugin.

Then, the vertical flow method is applied to determine the increase of the water table (h_e, (unit:

m)) associated with the event rainfall. Hence, the final position of the water table is the sum of the two increases of the water table. The equation to obtain h_a is expressed by:

$$h_a = \left(\frac{a}{b}\right)\frac{q_a}{Ksin\theta cos\theta}\left(\frac{\rho_w}{\rho_s}\right) \quad (2)$$

where a (m^2) is the drainage area, b (m) is the cell size, q_a (mm/d) is the effective antecedent water recharge, K (m/s) is the horizontal hydraulic conductivity (Montgomery and Dietrich, 1994a). The equation to calculate h_e (m) is as following:

$$h_e = \frac{P_e}{n} - \frac{(P_e-(5080/CN-51))^2}{n\cdot(P_e+4\cdot(5080/CN-51))} \quad (3)$$

where P_e (mm) is the event rainfall which represents the boundary condition for landsliding. n (-) is the soil porosity and CN (-) the curve number proposed in the event oriented SCS-CN model (USDA, 1986). SCS-CN is a hydrological model developed by the United States Department of Agriculture (USDA), and it is one of the simplest and most successful models in computing event-oriented runoff. CN is an empirical parameter used in the SCS-CN model for predicting direct runoff or infiltration from rainfall excess, and it only relates the runoff threshold and the soil water storage (USDA, 1986).

To remedy the issue regarding the uncertainty of soil property values, stochastic models (Simoni et al., 2008) have been proposed for the FSLAM, which allow the input parameters to have a statistical distribution within a range of possible values. Hence, when the inputs are in the form of stochastic parameters within a specific range, it is possible to compute the probability of failure (*PoF*) at each cell, which corresponds to the probability of having a *FS*-value lower than 1. Herein the parameters that can have stochastic inputs include two soil properties (C_s and φ), and root cohesion (C_r) related with Land Use and Land Cover (LULC) (Medina et al., 2021).

It must be stated that one of the limitations in the used stochastic model is using a normal distribution for the soil mechanical properties. However, beyond this limitation, another crucial assumption in Simoni et al. (2008) is that the variables are independent. This permits the problem to be analytically tractable, which is important for a simplified model.

2.1.2. Runoff modelling

The runoff module can be used to calculate the peak discharge at each cell following a rainfall event. For the plugin, this variable is not yet used to compute slope stability, but just to calibrate the

parameters by comparing its value to the observed hydrographs during the event. On the other hand, there are several mass movements related to in-channel processes, where the discharge is one of the main triggering mechanisms, hence in a near future, it is possible to include these processes into the model.

The curve number, which has been widely applied in hydrology, is the only parameter that is required in this phase (Yu, 1998; Woodward et al., 2002; Mishra and Singh, 2013). The approach to compute the peak discharge is the rational method, which requires the tributary area, the runoff coefficient and the rainfall intensity (Chow et al., 1988). The tributary area means the total area upstream of a specified point including all overland flow that directly or indirectly connects down-slope to this point, and it is calculated by applying a D8 cumflow algorithm (O'Callaghan and Mark, 1984). The runoff coefficient (*C*) is computed using the following equation (Témez, 1991):

$$C = \frac{(P_e - I_a)\cdot(P_e + 23I_a)}{(P_e + 11I_a)^2} \quad (4)$$

where I_a (mm) is the initial abstraction computed from the *CN* (-). Then, the rainfall intensity is computed using the Spanish Intensity-Duration-Frequency (IDF) curves (Témez, 1978):

$$I = I_d 11^{\left(\frac{28^{0.1} - T_c^{0.1}}{28^{0.1} - 1}\right)} \quad (5)$$

where *I* is the rainfall intensity (mm/d), I_d is the daily rainfall intensity (mm/h) measured as millimeters per hour, and T_c is the concentration time (h), which is expressed by:

$$T_c = 0.3\left(\frac{L}{j^{0.25}}\right)^{0.76} \quad (6)$$

where *L* (km) is the longest distance from the watershed divide to the outlet, and *j* (m/m) is the average slope.

By using the so-called *CN* method above, the FSLAM-plugin simplifies the event rainfall into two parts, namely the runoff and infiltration. The runoff calculation can be used for the calibration of the *CN*, whereas the infiltration is finally incorporated in the stability calculation.

2.2. Software design

2.2.1. General overview

A Graphical User Interface (GUI) was developed for the newest version of FSLAM code in order

to avoid the manual execution of the software. To facilitate this task, the well-known open source software QGIS was selected to implement FSLAM as a plugin (QGIS Development Team, 2021) because Geographic Information Systems (GIS) are the most common tools for the analysis of spatial data like landslide assessment. The plugin can be downloaded by the users, and even be improved including new functions beyond the current abilities.

An application named Qt Creator (https://www.qt.io/) based on Python language (https://www.python.org/) was selected to design and develop the interface of the FSLAM-plugin. Qt is a software development framework that can be used to develop applications on various operating systems.

The GUI connects the user with the different parts of the FSLAM-plugin (Figure 1). The three principal parts are: (i) input data, (ii) FSLAM model and (iii) output data. Details on the input and output data will be given later, but summarising, the input data include five raster and two text files, while the outcomes consist of 15 raster maps and 6 text files. In addition, the users can subsequently perform additional external analyses, e.g., the performance analysis by an existing landslide inventory.

Regarding the part of the FSLAM model, there are two main calculations, namely runoff and stability. In the runoff modelling, FSLAM starts with morphologic standard geoprocesses (fill sinks, slope calculation and flow accumulation, among others), and then calculates the infiltration and runoff. Regarding the stability modelling, the code mainly determines the following three conditions: (i) preliminary stability, (ii) initial stability considering the effective antecedent recharge, and (iii) final stability after event rainfall. It should be stated that new output files were added in the stability modelling of the plugin in respect to the original model presented by Medina et al (2021). These additional outputs improve the understanding of the infiltration and stability processes.

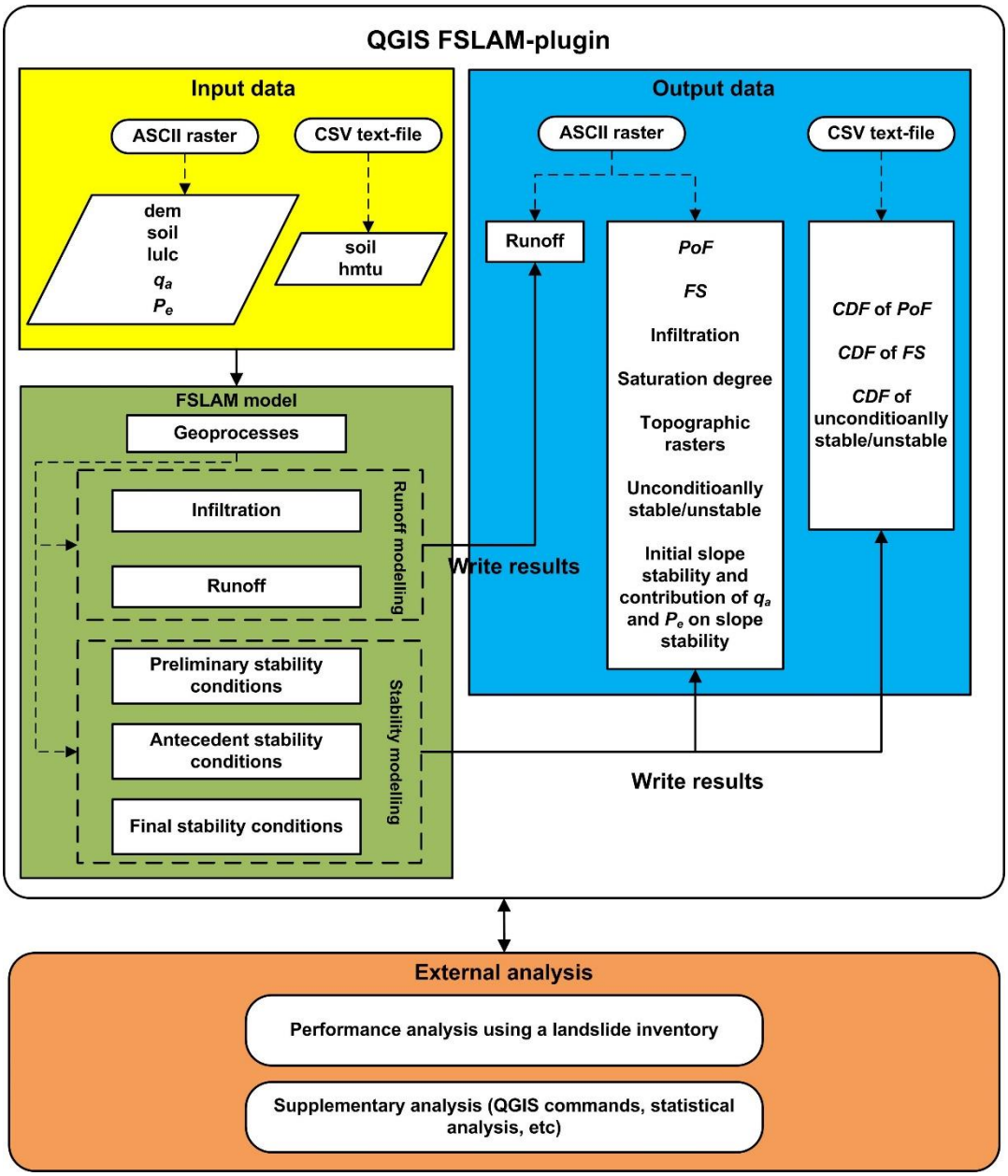

Figure 1 The work flow of the QGIS FSLAM-plugin. See text for more details of each part.

2.2.2. Computational requirements of FSLAM

The code of the FSLAM model is developed in Fortran 90 language, focusing on code performance. It is proposed as a model able to work at a regional scale but using small cell size.

The requirements in terms of RAM memory are high by the code, being the Flow Accumulation geoprocess the most demanding algorithm. Taking the case with 30 million cells as an example, the raster of the Digital Elevation Model (DEM) is stored in a 64 bits float number. Hence a 30 million DEM requires 458 MB of RAM. The Flow Accumulation algorithm multiplies this requirement eight times, resulting in up to 4 GB RAM. Additional storage is required for other float inputs, such as the

rainfall raster, slopes, etc, which raises this value by 8 GB of RAM. Land use and soils properties are stored as unsigned bytes in order to reduce the memory space but limiting the number of classes to 256. The 32 bits applications are limited to 2 GB of RAM, hence the code is developed in 64 bits. None OS specific functions are used. Therefore, the code could be compiled in any platform. Most of the algebraic operations take advantage of the vector parallelization provided by the compilers at instruction level. For iterative subroutines, OpenMP has been selected to explicitly parallelize algorithms. No MPI instructions have been used, hence it is not possible to take advantage of the HPC clusters.

2.3. Application and testing

The Berguedà region of Spain was selected as a test area in this study, in order to show the application of the FSLAM-plugin. This area has received an important interest after the catastrophic 1982 rainfall episode, which caused the most notable Multiple Occurrence of Regional Landslide Events (MORLE) in Eastern Pyrenees. This fact together with the availability of a landslide inventory and rainfall data make this case ideal for our purpose.

2.3.1. Study area and 1982 rainfall episode

The Berguedà study area is located in the southern side of the Oriental Pre-Pyrenees, NE Spain (Figure 2), and covers an area of 504.8 km^2. The region comprises the Upper Llobregat River (ULR) basin down to the La Baells water reservoir, which was inaugurated in 1976.

Geologically, the bedrock of the ULR basin consists of sedimentary rocks, including: limestones, conglomerates, mudstones, sandstones, and turbidites (Corominas and Moya, 1999; Bathurst et al., 2006). Besides, superficial alluvial and colluvial deposits of variable thickness, covering bedrock formations, are also found.

From a morphological point of view, the catchment elevation ranges from 622 m a.s.l up to 2500 m a.s.l at its highest point. The slope angles are mainly between 20º and 40º, being the inclination where more mass movements took place during the 1982 rainfall episode (Corominas and Alonso, 1990).

The Berguedà region has a Mediterranean climate, which is characterized by mild and wet winters,

along with hot and dry summers (Millán et al., 1995; Giorgi and Lionello, 2008). However, as other mountainous regions in the world, the orography and the south-facing location of the study area, introduce changes in the typical seasonal precipitation regimes (Trapero et al., 2013). In the Pyrenees, the collision between warm air masses coming from the south, and cold air fronts located beyond the mountain ranges can cause heavy precipitation, especially in the autumn when the Mediterranean Sea has warm temperature (Corominas and Alonso, 1990). If the total accumulated rainfall is equal to, or higher than 80 mm, they are considered torrential rains (Millán et al., 1995), and they can also be related to the occurrence of landslides (Corominas and Moya, 1999).

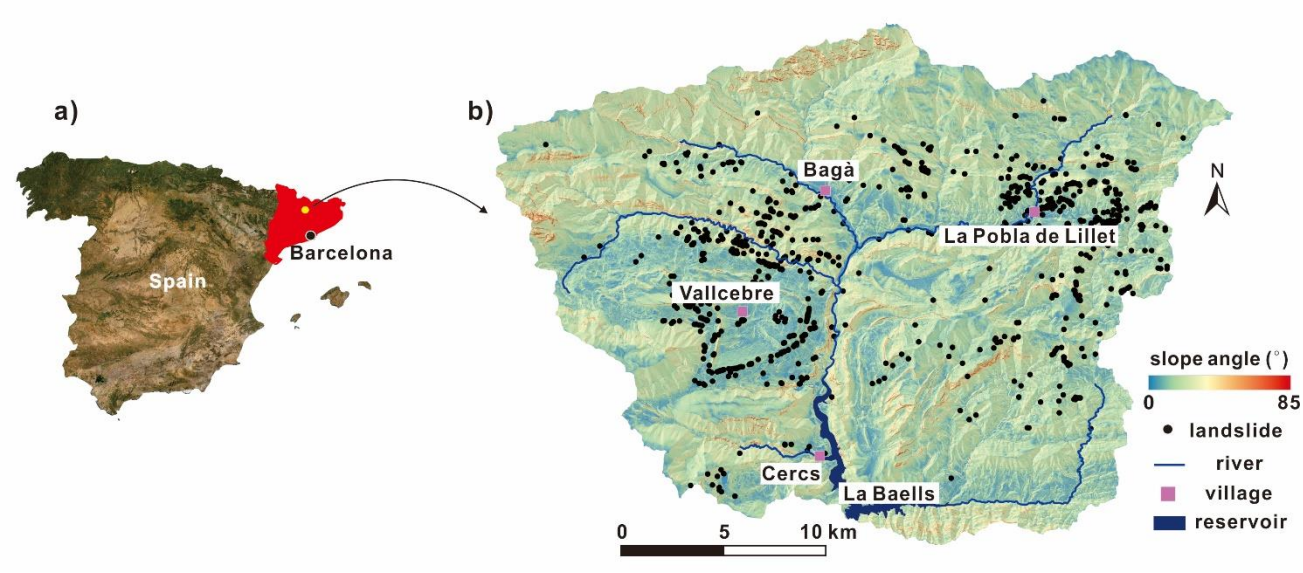

Figure 2 The Berguedà study area and the landslide inventory related to the 1982 rainfall episode: (a) Location of Berguedà (yellow dot) in the Pyrenees, and (b) the slope angle map generated from the digital elevation model with a resolution of 5 m.

From November 6 to 7, 1982, one of the most catastrophic and exceptional rainfall episode for the Eastern Pyrenees in the 20th century was recorded. A strong storm affected Spain, Andorra and France, reaching more than 400 mm of accumulative rainfall in a period of 24 h.

The consequences of this extreme weather episode were devastating. It triggered many slope instabilities and flash floods, causing 44 fatalities and considerable economic losses (Corominas and Alonso, 1990; Trapero et al., 2013).

The Berguedà region was severely affected by this rainfall episode and a large number of slope

failures were triggered. In particular, in a study area of 1250 km^2 more than 1800 mass movements were reported (Clotet and Gallart, 1984) including shallow slides, debris flows, slumps and rock falls. This number corresponds to a density of 1.5 movements per square kilometre. The area with a very high density of shallow landslides and debris flows was around Vallcebre and La Pobla de Lillet, where a total of 340 mm in 48 h was registered (Corominas and Moya, 1999; Bathurst et al., 2006).

The inventory that we used in this study includes shallow slides and debris flows associated with this catastrophic rainfall event. We merged inventories of previous studies (Clotet and Gallart, 1984; Baeza, 1994; Santacana, 2001), where the employed methods were mainly photointerpretation with aerial photographs and fieldwork. The total number of landslides in the final inventory was 998 (Figure 2), among which 11 points were inventoried by Baeza (1994), 157 by Clotet and Gallart (1984), 595 by Santacana (2001) and 235 by the Cartographic and Geological Institute of Catalonia (ICGC, 2021).

2.3.2. Available geospatial data

The FSLAM code applies the infinite slope theory and thus needs in every cell to solve the equations described in Section 2.1. These parameters, which are principally related to soil and LULC properties, are included in the five raster and two csv files that are required as the input data of the plugin (Figure 1).

The first input raster is the DEM (Figure 3a), which has continuous data type. It was downloaded from ICGC (2013) with a spatial resolution of 5 m. In the next step, the information on soil properties was approximated by the geological map at 1:50000 scale, as no geotechnical map was available. The geological map was downloaded from ICGC (2016) as a vector shapefile. Then, it was reclassified into thirteen lithological classes and transformed into a raster file with a 5 m resolution (Figure 3b). Given that the rainfall episode occurred in 1982, we used the oldest version of LULC map that exists from the study area, corresponding to the year 1987. A raster map was downloaded from the department of Territory and Sustainability with a spatial resolution of 30 m (ICGC, 2018). The original map had twelve classes that were reclassified into eight categories (Figure 3c) by combining some similar categories, and the resolution was resampled from 30 m into 5 m. It should be noted that the values in LULC and soil rasters are discrete data types which is different from the DEM raster. Different LULC and soil maps may have various categories and users are allowed to determine the exact categories in

LULC and soil rasters according to the situation of their study areas and data availability.

For all the parameters regarding soil properties and root cohesion required by the plugin, their initial values were selected by using standard literature, site-specific data and expert criteria (USDA, 1986; Baeza, 1994; ECORISQ, 2021; Geotechdata, 2021). Then, multiple FSLAM simulations were iteratively performed to fit the landslide episode that occurred in the Berguedà area in 1982. This step focussed mainly on the three most significant parameters of the FSLAM model (C_r, C_s and φ) (Medina et al., 2021) and calibrated them. In addition, the *CN* values were initially determined according to the ranges proposed by the Catalan Water Agency and the USDA (USDA, 1986; Montalbán et al., 2013). Subsequently, these values were calibrated by the runoff modelling where an iterative approach was also applied. Therefore, it is strongly recommended having an available landslide inventory and a known peak discharge data during the calibration procedure is also very useful. The calibrated parameters will be the best-fit values after the iterative FSLAM simulations. It must be stated that the plugin can also be used when no peak discharge data is available, since the runoff module is separated from the stability modelling. The final values of all the parameters obtained after the calibration phase for the Berguedà region are listed in Table 1 and Table 2.

In terms of precipitation, two raster files were used: one for the effective antecedent water recharge and another for the event rainfall. In general, the former can be determined by the regional average antecedent (e.g. monthly) rainfall and water balance data. The latter indicates the boundary condition for landsliding so it can be obtained from the storm event that triggers the landslide episode. In this study, the effective antecedent recharge map (Figure 3d) was determined using the official monthly precipitation maps published in the Catalan Climatic Atlas (GENCAT, 2008). The first five days of November (until the beginning of the triggering rainfall episode on November 6), no precipitation was measured in the Berguedà area, therefore the average monthly precipitation amount for October was used to determine the effective recharge. This map was adjusted by the precipitation observed during October 1982 at meteorological stations of the study area. On the other side, the event precipitation map was obtained by combining the isohyetal maps published by Hürlimann et al. (2003) and Bathurst et al. (2006) for the November 1982 event. Also, the simulation of a precipitation map of the 1982 rainfall episode carried out by Trapero et al. (2013), was included. Then, the isohyetal map

was adjusted using daily precipitation data that was recorded by the Spanish Meteorological Agency (INM) of the meteorological stations within the study area. Finally, the two maps were converted into the two necessary raster files with 5 m resolution (Figure 3e).

It is important to stress that we are trying to reproduce a real case study but the plugin could be easily used to try hypothetical scenarios (e.g. different rainfall events). Hence, it is possible to figure out the robustness of the model in the future since it can be expected that users would like to apply the plugin using a variety of different cases.

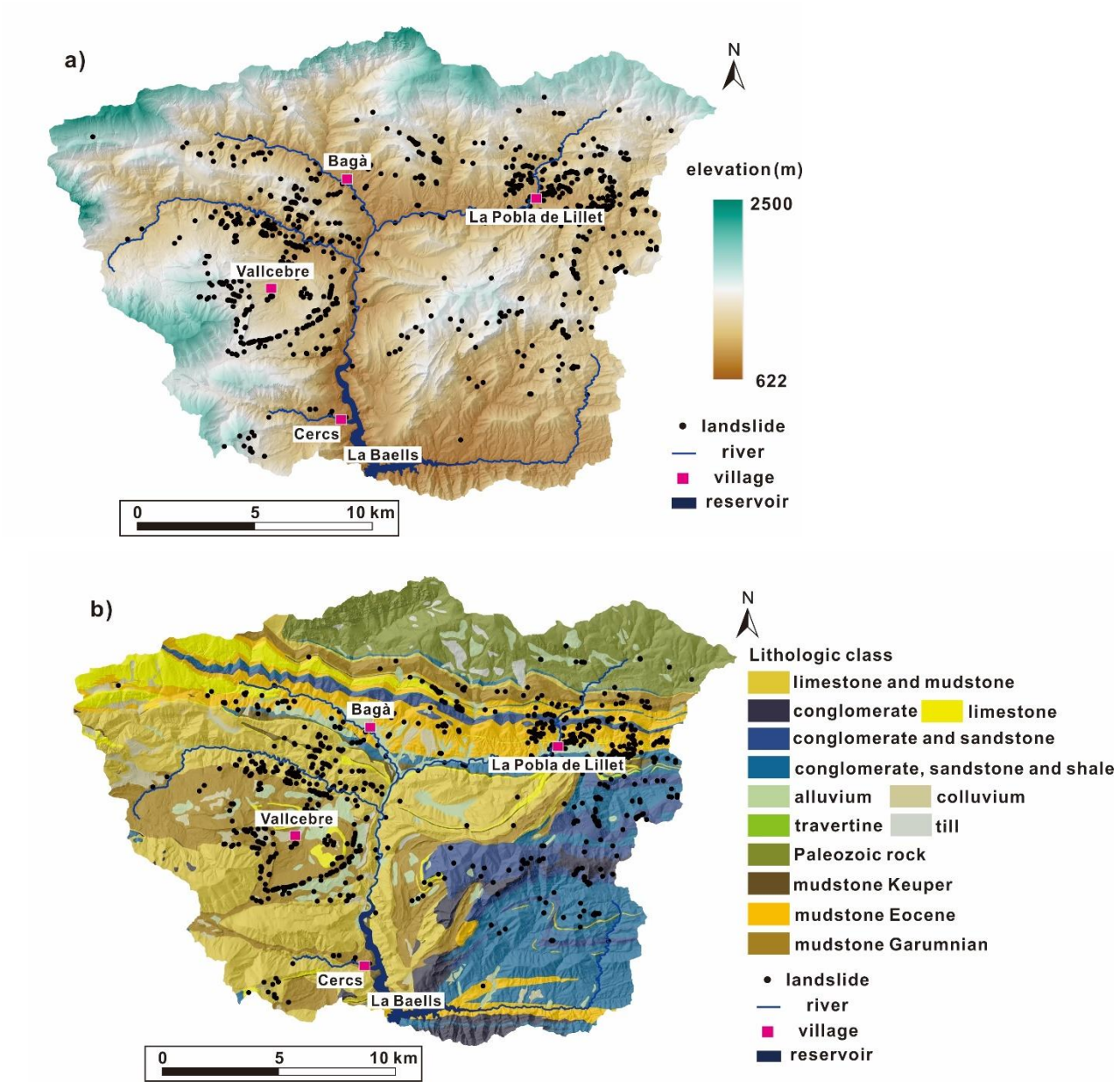

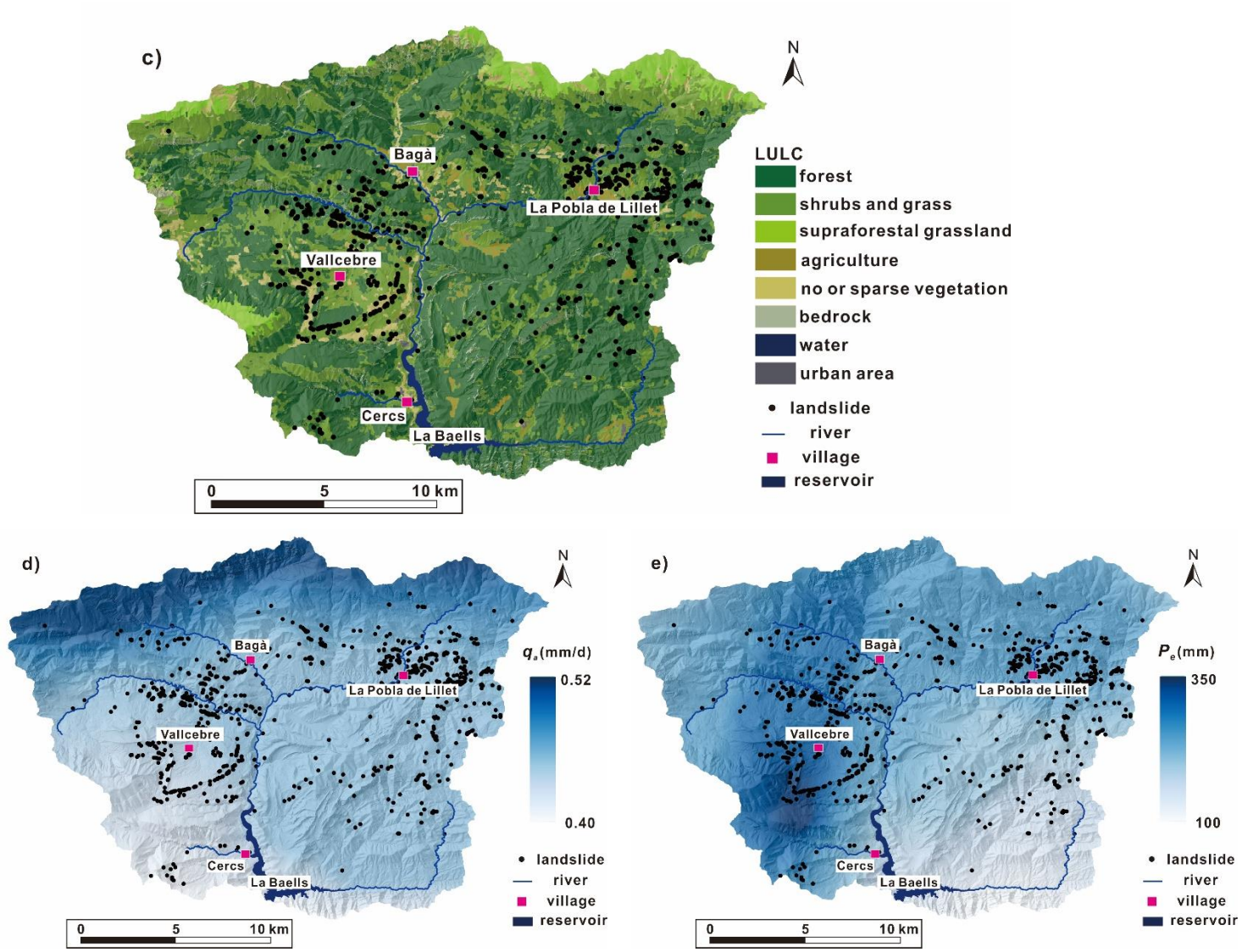

Figure 3 The five input raster maps of the Berguedà region for the FSLAM-plugin: (a) the DEM, (b) reclassified lithological map that provided the soil properties, (c) reclassified land use and land cover map, (d) effective antecedent recharge map, and (e) event rainfall map.

Table 1 Parameter values of the input text file called *"hmtu.csv"* including root cohesion (C_r), and the curve number (*CN*). The values are listed regarding the eight different LULC classes. SD stands for the standard deviation.

LULC	C_r-min/max (kPa)	C_r-mean (kPa)	C_r-SD (kPa)	*CN*-A (-)	*CN*-B (-)	*CN*-C (-)	*CN*-D (-)
forest	0/5	2.5	1.25	36	60	73	79
shrubs and grass	0/3	1.5	0.75	43	65	76	82
supraforestal grassland	0/2	1	0.5	49	69	79	84
agriculture	0/1	0.5	0.25	56	68	80	84
no or sparse vegetation	0/1	0.5	0.25	60	75	85	90
bedrock	999/999	999	0	77	86	91	94
urban area	0/1	0.5	0.25	90	92	96	98
water	999/999	999	0	100	100	100	100

Table 2 Parameter values of the input text file called "*soil.csv*" including soil properties related to the different lithological classes. HSG stands for hydrologic soil group (USDA, 1986, 2007).

Lithological class	C_s-min/max (kPa)	C_s-mean (kPa)	C_s-SD (kPa)	φ-min/max (°)	φ-mean (°)	φ-SD (°)	h (m)	K (m/s)	n (-)	ρ (kg/m^3)	HSG (-)
limestone and mudstone	0/3	1.5	0.75	20/30	25	2.5	1	10^{-5}	0.3	2000	B
limestone	0/5	2.5	1.25	35/45	40	2.5	1	10^{-5}	0.3	2000	A
conglomerate	0/4	2	1	30/40	35	2.5	1	10^{-2}	0.35	2000	A
conglomerate and sandstone	0/2	1	0.5	30/40	35	2.5	1	10^{-3}	0.35	2000	A
alluvium	0/2	1	0.5	20/30	25	2.5	1	10^{-2}	0.35	2000	A
colluvium	0/2	1	0.5	15/30	22.5	3.75	1	10^{-5}	0.3	2000	A
till	0/2	1	0.5	20/30	25	2.5	1	10^{-2}	0.35	2000	A
travertine	0/2	1	0.5	20/30	25	2.5	1	10^{-4}	0.3	2000	B
Paleozoic rock	0/3	1.5	0.75	25/35	30	2.5	1	10^{-2}	0.3	2000	B

mudstone Keuper	0/4	2	1	15/25	20	2.5	1	10^{-5}	0.3	2000	B
mudstone Eocene	0/4	2	1	15/25	20	2.5	1	10^{-6}	0.3	2000	B
mudstone Garumnian	0/4	2	1	15/25	20	2.5	1	10^{-6}	0.3	2000	B
conglomerate, sandstone and shale	0/2	1	0.5	30/40	25	2.5	1	10^{-4}	0.35	2000	A

2.3.3. Analysis of the landslide inventory

In order to reveal the main factors affecting slope failures in the study area, the relationship between landslide and different governing factors was analysed, including elevation, slope angle, lithological class and LULC. The slope map was derived from the DEM raster with 5-m resolution. We counted the total number of landslides in each category and also computed the density of landslides (number of landslide inventory points per square-kilometre) (Figure 4). The analysis of the morphologic factors showed that the landslides mainly occurred at low-medium elevations (Figure 4a). The elevations between 800 and 1600 m asl identify most landslides in the region and also have the peak of density of landslides. A majority of landslides started at the slope angles ranging from 25 to 40°, whereas the areas with slope angles between 35 and 45° have the peak of density (Figure 4b). The similar finding has also been revealed in other previous studies (Hürlimann et al., 2016; Shu et al., 2019), namely slope angle plays the most important role in landslides in the Pyrenees.

Regarding the lithological class (Figure 4c), the category of mudstone (Garumnian, Eocene and Keuper) contributes most to the landslide occurrence, followed by limestone and mudstone; conglomerate, sandstone and shale; alluvium, and limestone. Except these classes, the numbers of landslides in the other classes were much smaller. Finally, the effect of LULC on landslide initiation (Figure 4d) indicated that nearly 90% of the landslides started in forest, shrubs and grassland. Additionally, the category of bedrock is another significant LULC category with a large value of density.

Overall, all these factors mentioned above have contribution to landslide initiation in the

Berguedà region, because the spatial landslide distributions in different categories of each factor show evident difference. Therefore, it is necessary to incorporate this information into the model.

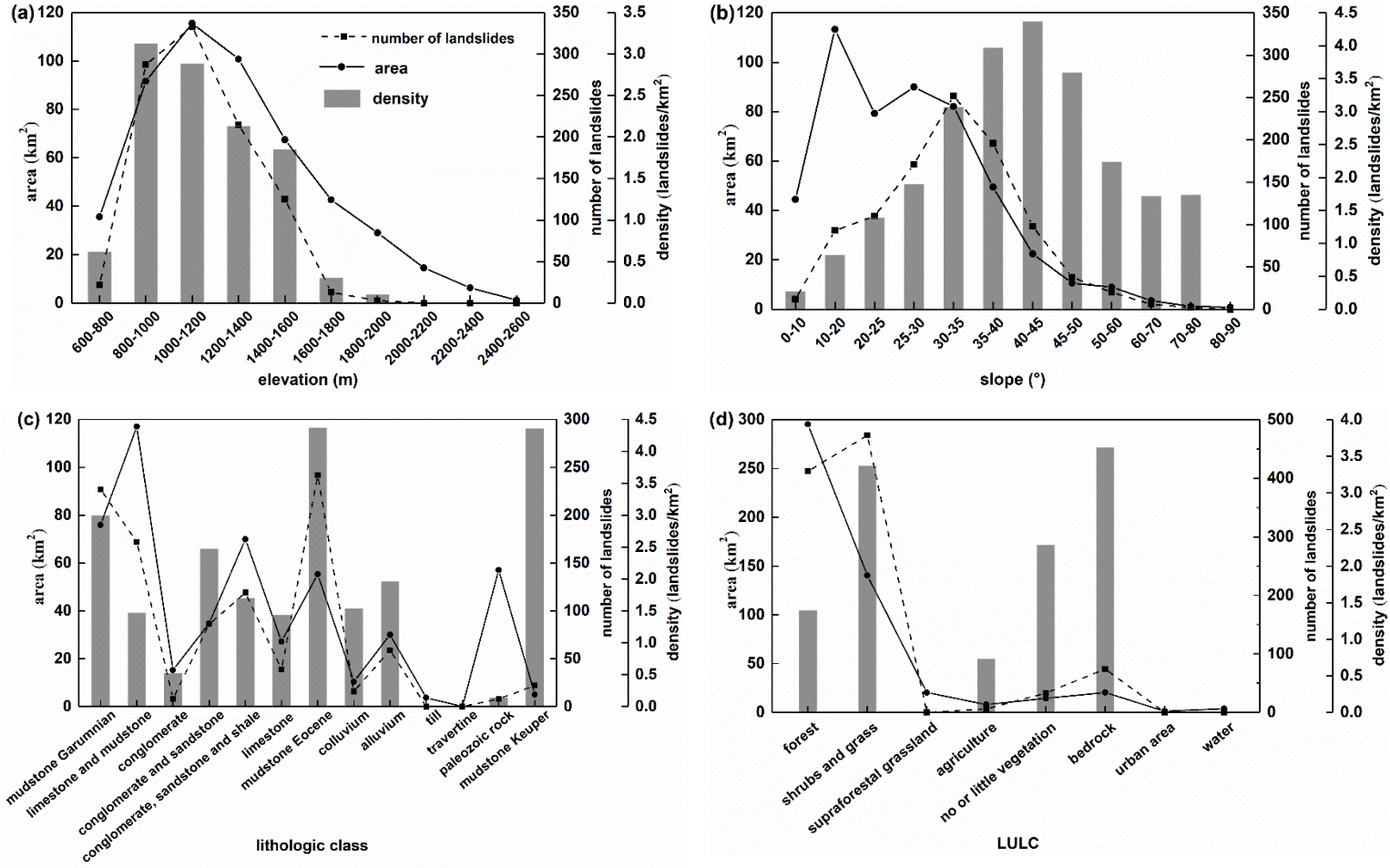

Figure 4 Analysis of effects of some governing factors on the Berguedà landslide inventory points: (a) elevation, (b) slope, (c) lithologic class, and (d) LULC.

2.4. Performance analysis of landslide susceptibility mapping

Performance analysis is not a built-in function of the FSLAM-plugin, but can provide insights into the results of the landslide susceptibility mapping. In this study, three methods were applied to evaluate the performance of the landslide susceptibility map generated by the FSLAM-plugin.

First, 5000 points were randomly selected within the study area, and their *PoF* values were compared with the landslide inventory points in the region. Three rainfall scenarios were considered, namely no rainfall, only q_a, and q_a and P_e. The comparison of *PoF* values between inventory and

random points can reveal the effects of rainfall conditions on the slope stability.

Second, the receiver operating characteristic (*ROC*) analysis (Fawcett, 2006) was used to evaluate the model accuracy. The *ROC* curve is a widely used approach which can display the results of a binary classification between the outcomes of a predictive model and the actual occurrence of the forecasted event (Corsini and Mulas, 2017). Here, the area under the curve (*AUC*) is used to indicate the model performance, and a higher *AUC* value represents a better result.

When a physically-based model is applied to evaluate the slope stability, it is necessary to appropriately determine a threshold for the safety level of the slope. Hence, in the last step, the confusion matrix under a specific classification threshold was provided to understand the model performance. According to previous literature (Silva et al., 2008; Park et al., 2013; Lee and Park, 2016), the *PoF* of 0.1 was selected as the threshold for safety level of natural slopes in probabilistic analysis of this study. Different indexes were counted including true positive (*TP*), true negative (*TN*), false positive (*FP*), false negative (*FN*), true positive rate (*TPR*), false positive rate (*FPR*) and accuracy (*ACC*). The relative trade-off between *TPR* and *FPR* was also plotted into the *ROC* curve to calculate the distance from the model result to the perfect classification. The so-called perfect classification would be located at the upper left of the *ROC* curve with the coordinate of (0, 1) (Park et al., 2013).

3. Results

3.1. Plugin implementation results

3.1.1. Plugin overview

After downloading the plugin, the whole plugin folder should be copied to the installation directory of QGIS plugins before it can be used. The installation process is swift, followed by the manual activation by using the "Manage and Install Plugins" window under the "Plugins" menu in QGIS. Then the FSLAM plugin can be launched from its toolbar within QGIS, or it can be directly opened by the icon on the menu.

Once the plugin is executed, the Graphical User Interface (GUI) of the FSLAM-plugin appears (Figure 5), which includes four tab widgets, named "*Inputs*", "*Outputs: runoff*", "*Outputs: stability*" and "*Info*". The input and output data are determined in the first three tabs and the last one shows the

1 plugin information (the model description, logo, and references used in the plugin). More details on
2 the requirements and limitations related to these tabs are described in continuation.
3

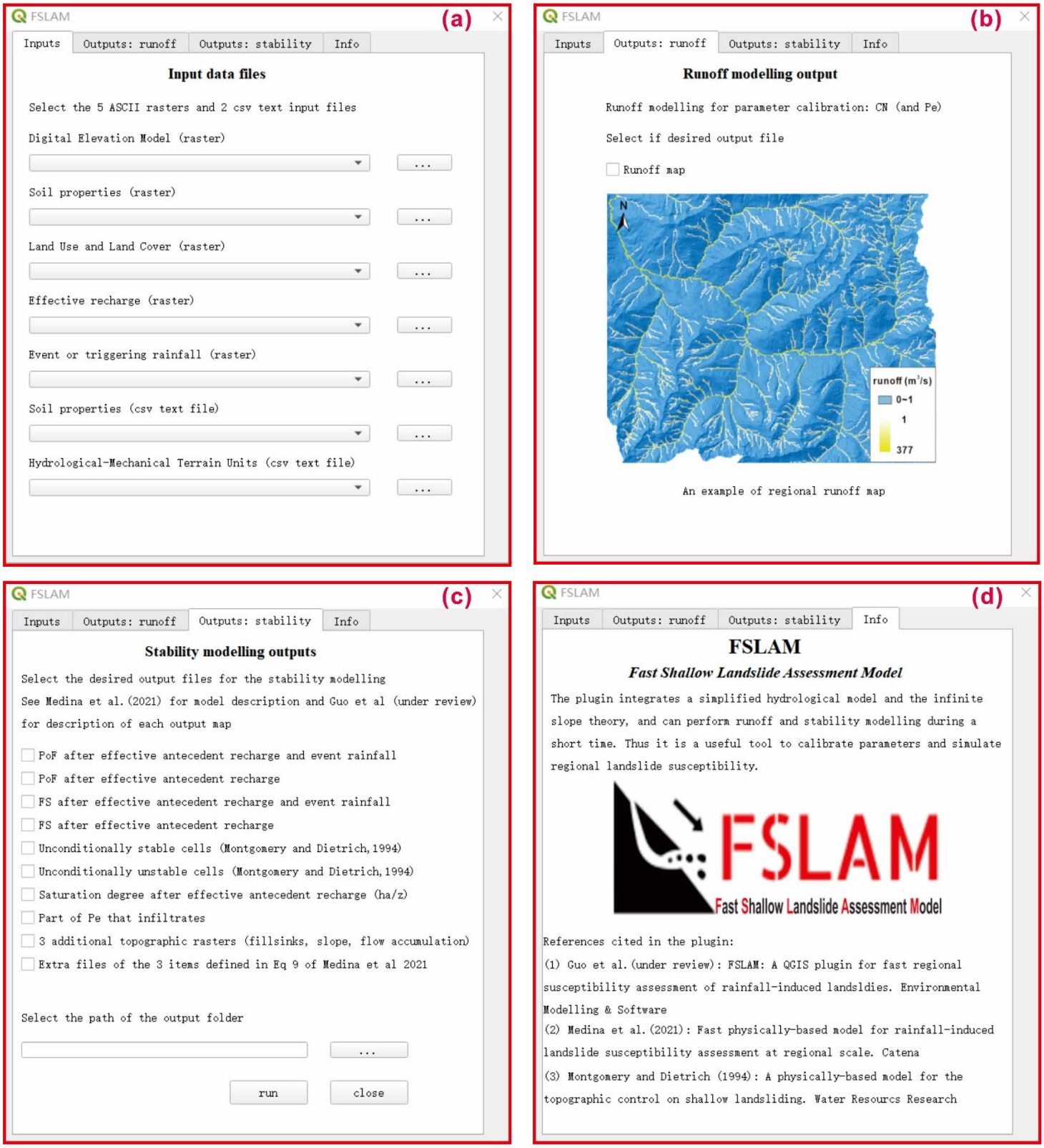

Figure 5 Four tabs of the FSLAM-plugin: (a) The "*Inputs*" tab showing the required input files, (b) The "*Outputs: runoff*" tab which allows users to select the runoff map as the output of runoff modelling, (c) The "*Outputs: stability*" tab where users can select the desired outputs for the stability modelling, and (d) the "*Info*" tab presenting some basic information of the plugin.

3.1.2. Input data

In the "*Inputs*" tab, it is required to load all the input files for the FSLAM model, including five ASCII raster files and two csv text files (Figure 1).

The raster files are the digital elevation model, the soil properties, the land use and land cover, the effective antecedent recharge, and the event rainfall. Three of them are continuous raster files and have units, namely DEM in m, effective recharge in mm/d, and event rainfall in mm. The other two raster files (soil and LULC) are categorical and theirs positive integer values are linked to the two csv text files that include the parameter values of each specific soil or LULC category. Specifically, for each identified category in LULC and soil rasters, the algorithm built-in the plugin seeks the parameters that are used for the model calculation in the corresponding text files. Next, these parameters will be linked into the rasters to carry out modelling.

The first text file includes the six soil properties (soil cohesion, friction angle, soil depth, hydraulic conductivity, porosity and density), and the hydrologic soil group (*HSG*) (USDA, 1986, 2007) for each soil class. The second file describes the hydrological-mechanical terrain unit (*HMTU*), and provides the values of root cohesion and curve number (*CN*) for each LULC category. All the parameters in these two text files can be stochastic. When more than two stochastic parameters are involved in the analysis, the Monte Carlo simulation may be a better option for the probabilistic analysis since it can consider many other probability distribution functions, but it would strongly increase the computational time (Simoni et al., 2008; Medina et al., 2021).

Additionally, it should be noted that all the raster maps must have the same format, spatial extent, pixel size, coordinate system and no data value. Hence, it is highly recommended to align all the raster files by using the "*Align raster*" tool in QGIS before using them as inputs. Based on our experiences, no data should be determined as a specific value, which must be different from the other values in the input rasters (e.g. -9999). QGIS tool can be used to reproject to a different coordinate system, change

the no data value or to resample pixel size. However, the resolution of the original raster will impact on the results, as well as the uncertainty of the input data will change with pixel size.

3.1.3. Output data

The output data of the plugin can be selected in the "*Outputs: runoff*" and "*Outputs: stability*" tabs. Only one raster file can be obtained from the tab of "*Outputs: runoff*", named *runoff.asc*, which shows the peak discharge in each cell. The stability modelling offers 14 raster files regarding multiple data for analysis. For the raster files in these two tabs, every item is optional, but at least one file should be selected as the output, otherwise the model runs but no output data are given. Additionally, for the first six checkboxes in the "*Outputs: stability*" tab, an extra csv file will be generated for each of the selected option. These text files contain data on the cumulative distribution function (*CDF*) of the resulting raster files. The name of the csv files is the same as the corresponding raster file, followed by the suffix "_CDF". All the output files (raster and text files) related to the tab of "*Outputs: stability*" are listed in Table 3.

Table 3 Description of the output files in the FSLAM-plugin

Plugin checkbox in the tab of "*Outputs: stability*"	File name in the output folder (unit)
PoF after effective antecedent recharge and event rainfall	PROB_failure_final_cond.asc (-) PROB_failure_final_cond_CDF.csv (-)
PoF after effective antecedent recharge	PROB_failure_ant_cond.asc (-) PROB_failure_ant_cond_CDF.csv (-)
FS after effective antecedent recharge and event rainfall	FS_final_cond.asc (-) FS_final_cond_CDF.csv (-)
FS after effective antecedent recharge	FS_ant_cond.asc (-) FS_ant_cond_CDF.csv (-)
Unconditionally stable cells (Montgomery and Dietrich, 1994b)	PROB_uncond_stable.asc (-) PROB_uncond_stable_CDF.csv (-)
Unconditionally unstable cells (Montgomery and Dietrich, 1994b)	PROB_uncond_unst.asc (-) PROB_uncond_unst_CDF.csv (-)
Saturation degree after effective antecedent recharge (h_a/z)	h_z_ant_cond.asc (-)
Part of P_e that infiltrates	Infiltration.asc (mm)

3 additional topographic rasters (fillsinks, slope, flow accumulation)	fill.asc (m) slopes.asc (rad) cumflow.asc (m^2)
Extra raster files of the 3 terms defined in Eq 9 of Medina et al 2021	FS_event.asc (-) FS_antecedent.asc (-) FS_dry.asc (-)

Users can assign any existing folder in their computer as the path to store the output files. All the selected output raster files as well as the corresponding csv files will show up in this output folder. Additionally, a text file named filenames.txt that contains the path of all input files, is created, which can be used for future consultations of the simulations performed.

In the following, the 14 outputs regarding the stability calculations will be described. The first two outputs are related to the probability of failure (*PoF*). If the first checkbox "PoF after effective antecedent recharge and event rainfall" is selected, the plugin computes the raster map called "PROB_failure_final_cond.asc", which includes the *PoF* value at each cell after applying q_a and P_e, whereas the *PoF* value after q_a can be generated by using the checkbox of "PoF after effective antecedent recharge". Both maps have a range from 0 to 1. The effect of the event rainfall on slope stability can be identified by comparing the two maps. Meanwhile, the *PoF* map after q_a can indicate the impact of the effective antecedent recharge on slope stability, when compared with the *PoF* map under dry conditions.

The following two outputs calculate the Factor of Safety (*FS*) under the same conditions as for *PoF*: (i) applying q_a and P_e, and (ii) applying only q_a. The values in both maps are larger than 0, and the two maps can be used to check unstable areas with *FS* values less than 1.

The next two checkboxes related to definitions proposed by Montgomery and Dietrich (1994b). The checkbox "Unconditionally stable cells" shows the stability condition of each cell when the soil is completely saturated. Specifically, it indicates the probability of each cell of being unconditionally stable (*PoUS*), hence mathematically the value equals to the difference between 1 and the *PoF* under saturated condition. If some landslide points with high *PoUS*-values are located in the area, it means that the soil properties must be checked, because even with fully saturated soil, the soil will be stable.

The checkbox of "Unconditionally unstable cells" indicates the *PoF* at each cell when soil is completely dry. It can also be explained by the probability of being unconditionally unstable (*PoUU*) of each cell. If no landslide points in the area with high *PoUU* values, the areas where the landslide points start may have too large soil property values, thus the soil properties must be checked in this condition. In areas where slopes are very steep it could happen that values of *PoUU* are inevitably very high. This could only be avoided by giving soil properties of bedrock instead of soil.

The following two outputs are associated with the saturation and infiltration. The checkbox "Saturation degree after effective antecedent recharge (h_a/z)" computes the raster file named "h_z_ant_cond.asc", which shows the position of the water table in relation to the depth of the soil layer after the effective antecedent recharge. It equals to the ratio between the increase of the water table associated with the effective antecedent recharge (h_a) and the soil depth (z). The raster file named "Infiltration.asc" is generated from the checkbox "Part of P_e that infiltrates", and it shows the amount of event rainfall, which infiltrates into the soil layer. The remaining part of the event rainfall is surface runoff, which results in the peak water discharge.

The FSLAM-plugin also provides topographic outputs by the checkbox "3 additional topographic rasters (fillsinks, slope, flow accumulation)". These outputs include: (i) the DEM with the sinks filled (fill.asc); (ii) slope angle map derived from the DEM (slope.asc), and (iii) the map showing the drainage area at each cell (cumflow.asc).

Finally, three additional outputs can be obtained by selecting the checkbox "Extra raster files of the 3 terms defined in Eq 9 of Medina et al 2021". These three raster files are containing data on the initial stability conditions (e.g., slope, cohesion, thickness, etc) and the influence of q_a and P_e on the slope stability. The contributions of both effective recharge and event rainfall to *FS* are not larger than 0, while that of the parameters under dry conditions is not less than 0. The equations of these three contributions are given in Eq. 9 of Medina et al (2021).

The path for the outputs can be set by clicking the combo box above the "*run*" button.

3.2. Testing results

3.2.1. Computing time

All the raster files were prepared at a 5 m resolution, which gives a total of about 30 million cells for the entire Berguedà study area. Simulations showed that the stability calculation of the FSLAM-plugin only lasted approximately 4 minutes for the entire region. However, a comparison of computing time showed that the writing of rasters files lasted much longer than the stability calculations. Hence, the entire run of the plugin including the writing of all the raster files lasted approximately 80 minutes. This leads us to conclude that it is important to determine which outputs are required for the analysis before applying the plugin, since this choice can strongly reduce the running time of the plugin. All the calculations above were performed by a computer with one 8-cores 1.8 GHz *CPU* and 8 GB of *RAM*.

3.2.2. Output results

When selecting all the checkboxes in the GUI, the plugin will write fifteen raster maps and six csv text files in the specified result folder. In the following, the raster maps are divided into three groups namely hydrological maps, *FS*-related maps and *PoF*-related maps. The only two maps that will not be shown are the filled DEM (fill.asc) and slope map (slope.asc), since the slope map has already been presented in Figure 2.

As stated above, the runoff map (Figure 6a) was used to calibrate the curve number by comparing the observed and computed peak discharge. The observed peak discharge into the La Baells reservoir was estimated as 1300 m^3/s (C. Barbero, Catalan Water Agency, personal communication, March 15, 2021), whereas the simulated runoff by the plugin was 1394 m^3/s (Figure 6b). The error between simulated and actual values of runoff was only approximately 7%, which is satisfactory for such a simplified approach and the existing uncertainties of P_e and *CN*. However, this runoff modelling indicates that the selected *CN* values (Table 1) fit well for hydrologic conditions of the 1982 rainfall episode.

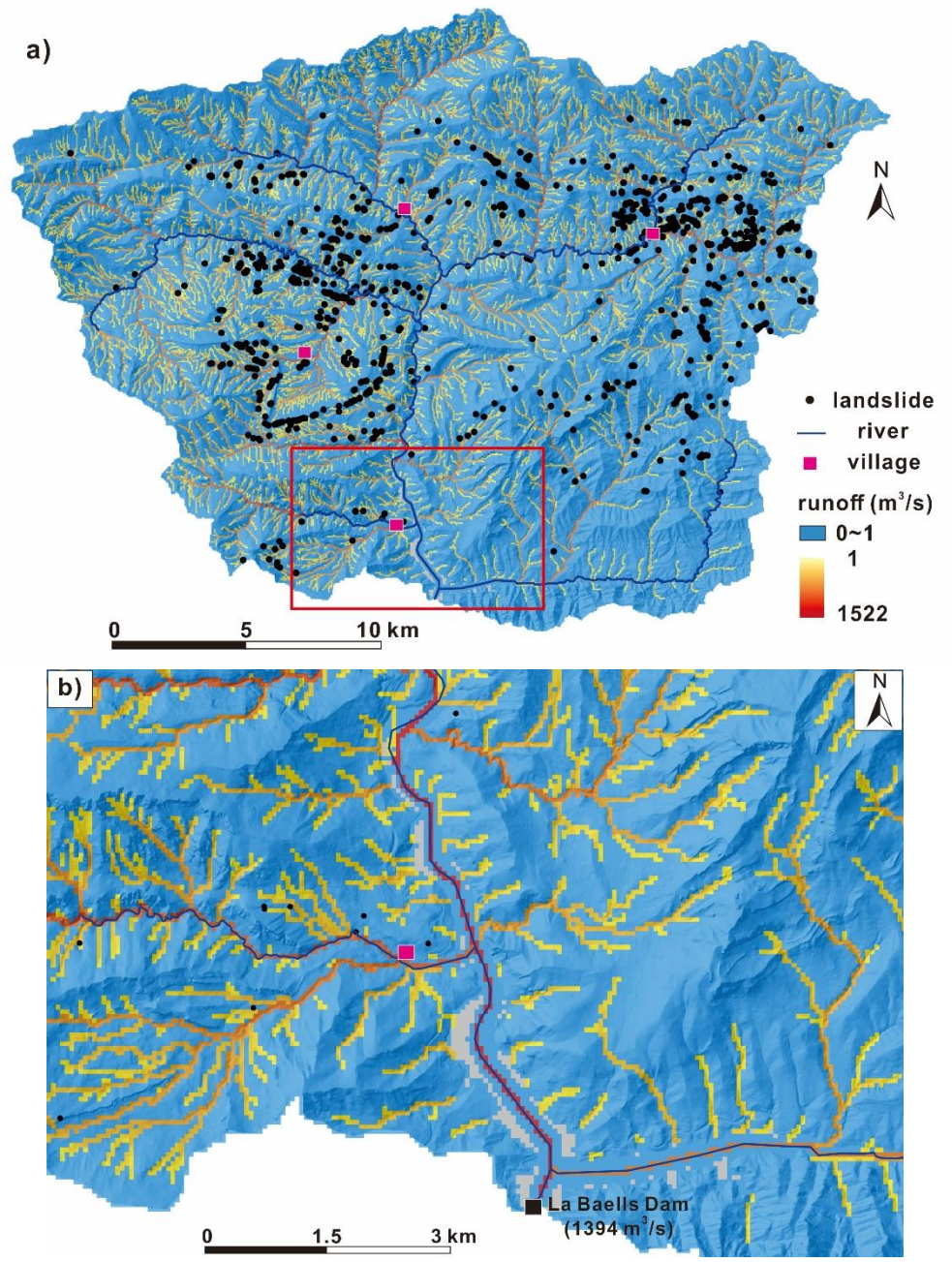

Figure 6 Runoff map for the 1982 rainfall episode, which was used for the calibration of *CN*. The red rectangle in (a) shows the exact location of the zone in (b).

In addition to the runoff map, the first group of outputs of the FSLAM-plugin includes the flow accumulation map, infiltration map, and relative saturation degree map. They are all hydrology-related maps and are useful to understand the infiltration processes during a rainfall episode.

The flow accumulation map (cumflow.asc) (Figure 7a) is not only directly related to runoff, but also to h_a. The flow accumulation values range up to 10^7 m^2 in the Berguedà area. We can see that

ridgelines mostly have smallest values, and maximum values are mainly located at valley floors where main river are situated.

The infiltration map (Infiltration.asc) (Figure 7b) shows the potential amount of the event rainfall, which may infiltrate into the soil. In the Berguedà area, it ranges from 0 to 255 mm. Relatively large values of infiltration (more than 170 mm) mainly occur in the lithological classes with high porosity. On the contrary, the lithological classes with low porosity (for example mudstones) have small infiltration.

The map showing the relative saturation degree applying the effective antecedent recharge (h_z_ant_cond.asc) is related to the flow accumulation and the hydraulic conductivity (Figure 7c). Because the hydraulic conductivity is linked to the lithology, high percentages of relative saturation degree (more than 0.75) mainly occur in mudstones, where *K*-values are low. On the contrary, conglomerate, sandstone and alluvial lithologies are less saturated due to their relatively high hydraulic conductivity.

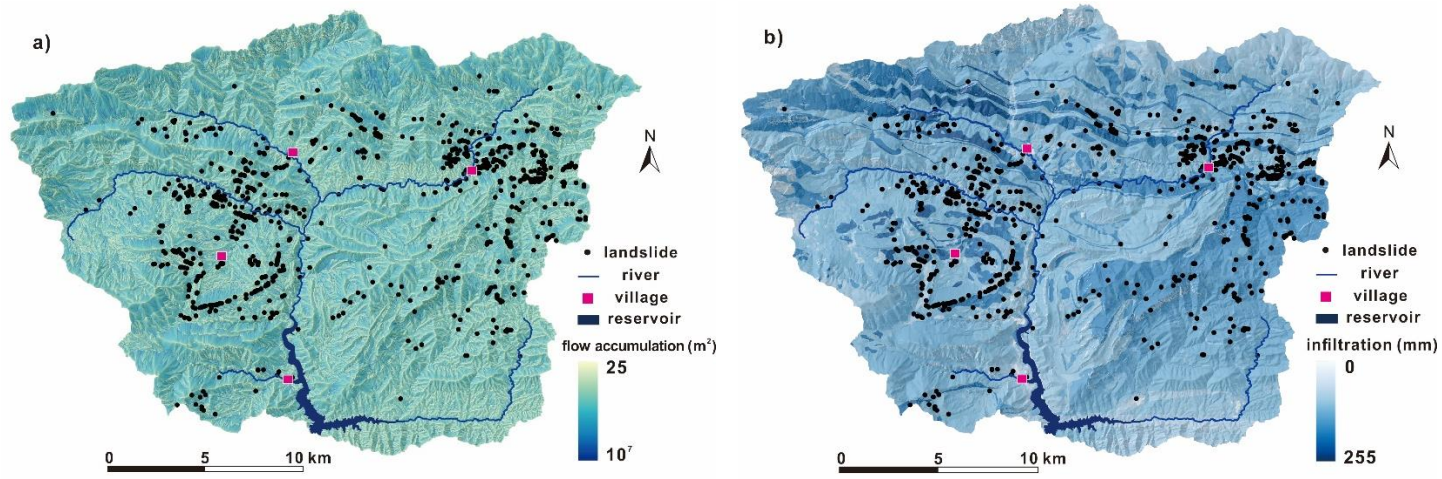

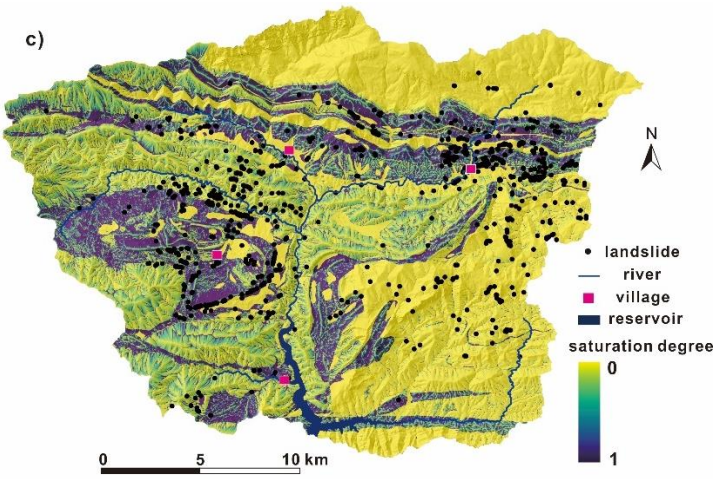

Figure 7 Output maps related to the hydrological modelling of the FSLAM-plugin: (a) flow accumulation, (b) part of event rainfall that infiltrates into soil layer, and (c) relative saturation degree after effective antecedent recharge.

The second group of outputs is composed of five maps related to the factor of safety (FS) and generated from the stability modelling. They reflect the stability conditions in the study area under different rainfall scenarios using the mean parameter value in the range of the stochastic model.

The raster maps named "FS_ant_cond.asc" (Figure 8a) and "FS_final_cond.asc" (Figure 8b) show a clear correlation between the slope angle and the stability, since in those areas with smooth slopes, the safety factor is evidently higher. When only the effective antecedent recharge is considered, most zones in the study area are stable, especially in the areas with a low saturation degree of the soil layer (see Figure 7c).

The specific effects of the two rainfalls and the soil properties under dry conditions, can be identified and compared using the other three maps in this group. The contribution of the effective recharge (Figure 8c) is closely related to the hydraulic conductivity and thus with the lithological classes. In a similar way to the saturation degree map, those areas with mudstone type-lithology are mostly affected by the effective antecedent recharge. In other areas, the decrease of *FS* is associated with the infiltration of the event rainfall (Figure 8d). Rainfall conditions can decrease the slope stability so the contributions of both q_a (Figure 8c) and P_e (Figure 8c) to *FS* are negative values.

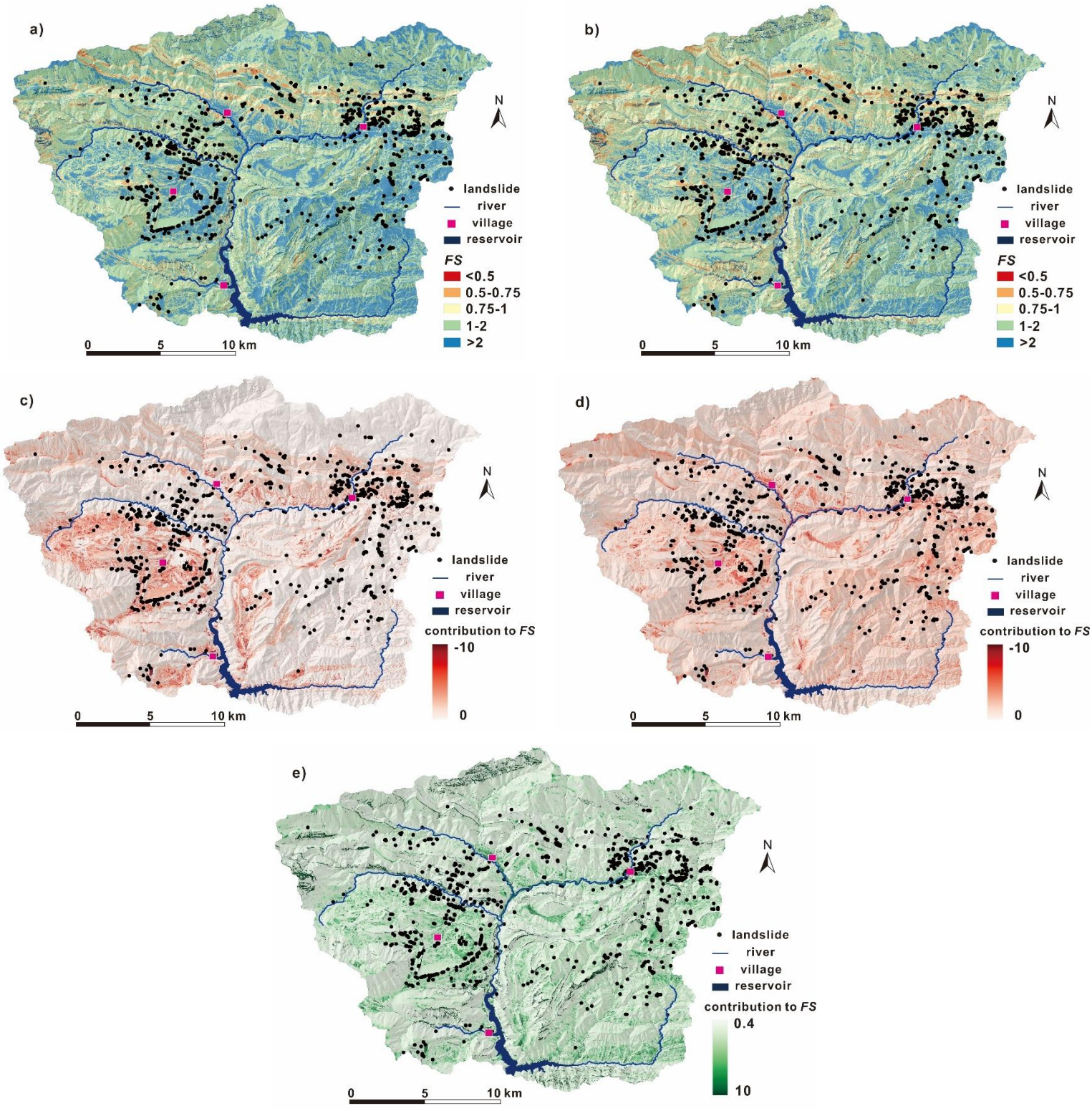

1 Figure 8 *FS*-related output maps from stability modelling of the FSLAM-plugin: (a) *FS* after effective
2 antecedent recharge, (b) *FS* after effective antecedent recharge and event rainfall, (c) contribution of
3 effective antecedent recharge to *FS*, (d) contribution of event rainfall to *FS*, and (e) contribution of
4 parameters under dry conditions to *FS*.

The third group of output files are *PoF*-related maps and show the probability of failure for different rainfall and soil saturation scenarios. They are key outputs of the FSLAM-plugin as they show those areas most likely to generate landslides and, therefore, they allow the users to anticipate and perform a good risk management.

Overall, the study area is stable when only the effective antecedent recharge is applied (Figure 9a). Most areas with *PoF* values larger than 0.75 occur in the Garumnian and Eocene mudstones. After the event rainfall, the stability condition in many areas greatly decreases (Figure 9b). This indicates that the input of the event rainfall makes these cells to reach the critical stability conditions.

The *PoUS* values under totally saturated condition, have a high relationship with slope angle in the study area (Figure 9c). In comparison to steep slopes, it is evident that relatively flat areas have larger probability to be unconditionally stable. For example, the valley floors generally have high *PoUS* values, which indicates that the *PoF* at these areas is low or even negligible. On the contrary, the value of 0 (i.e., *PoF*=1) reveals those areas that have the highest landslide susceptibility under totally saturated condition. Many landslide inventory points are located in such areas, indicating that the soil properties used are appropriate. Regarding the *PoUU* map under dry conditions (Figure 9d), it may have minor importance because most of the areas in Berguedà have low values. To properly distinguish these two maps, it is important to understand that an equal value on both maps, represents totally opposite meanings. For example, *PoUS* = 1 stands for a cell that is always stable even in totally saturated condition, while *PoUU* = 1 means that the cell is always unstable, even without any rainfall.

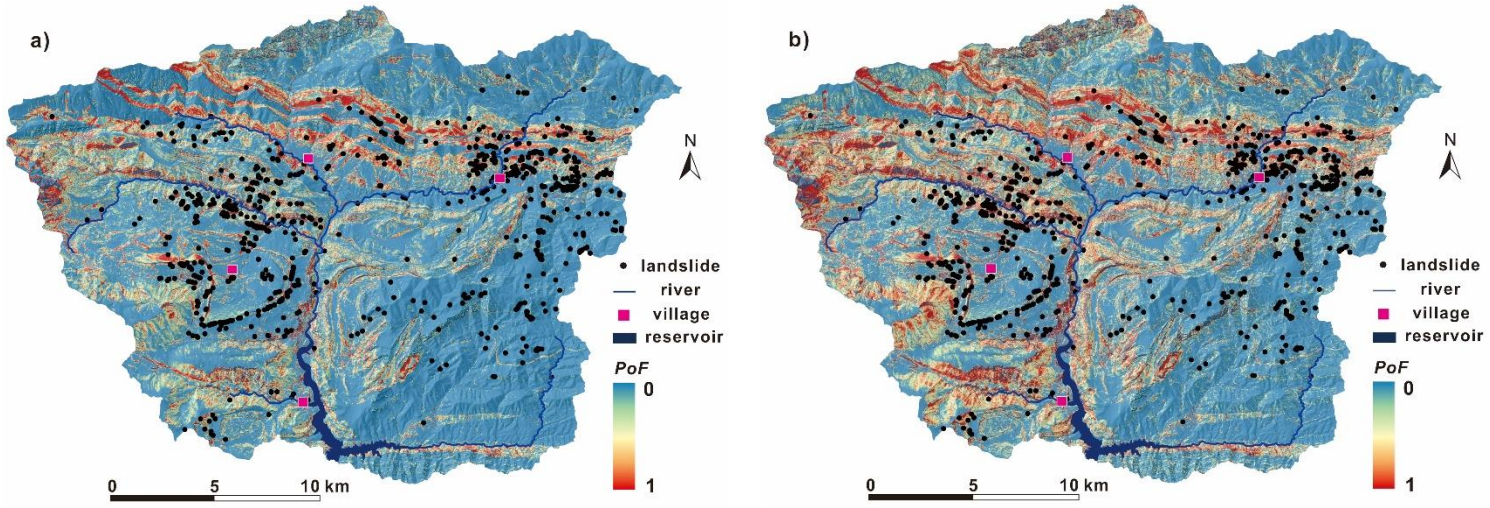

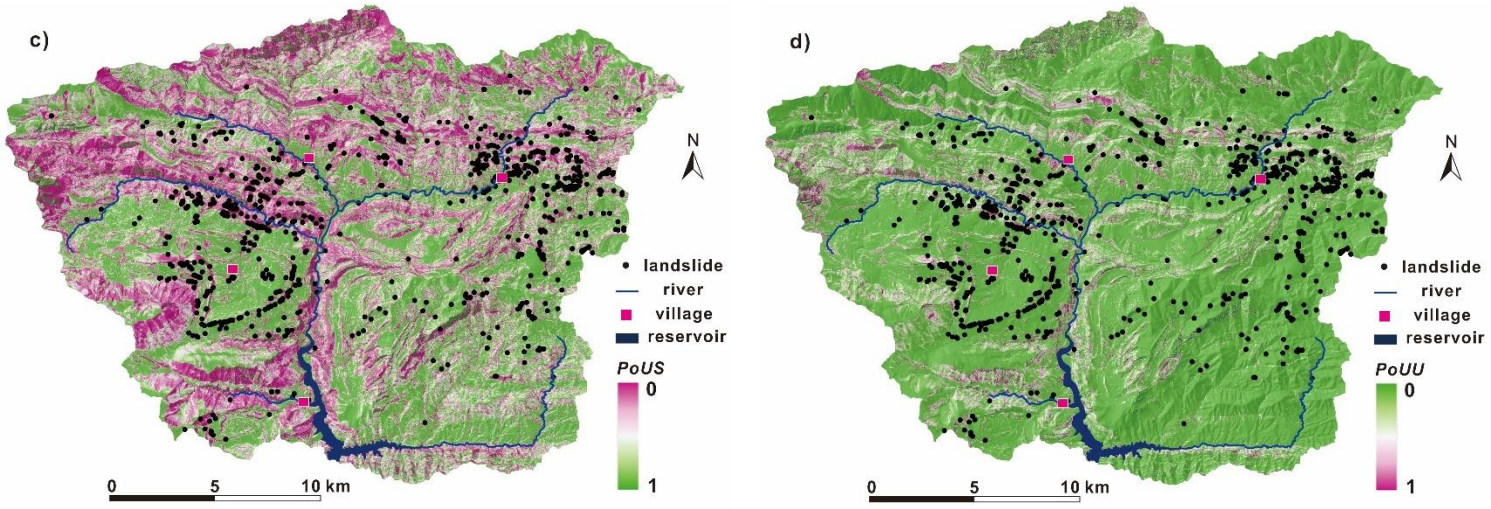

Figure 9 *PoF*-related output maps from stability modelling of the FSLAM-plugin: (a) *PoF* after effective antecedent recharge, (b) *PoF* after effective antecedent recharge and event rainfall, (c) *PoUS* under totally saturated condition, and (d) *PoUU* under dry condition.

In addition to the maps showed above, the FSLAM-plugin also calculates csv text files outputs. They can be simply presented as curves plots, which should help the interpretation of the maps (Figure 10). We have grouped the curves with the same topic into one plot, in order to be able to better compare them. Considering that the range of *FS* at regional scale may be very large, the csv files only lists the cumulative distribution function (*CDF*) when *FS* is not larger than 1.

The comparison under different rainfall conditions (Figure 10a), reveals the negative effect of the event rainfall on slope stability. For instance, after the q_a only 17% cells are unstable (*FS*<1), but the percentage increases to 27% after applying q_a and P_e. Additionally, regarding the *CDF* curves of the *PoF* values under different rainfall conditions (Figure 10b and Figure 10c), the overall stability condition can be revealed and compared by computing the area under the *CDF* curve (AUC_{CDF}). The larger the AUC_{CDF} is, the more stable the study area is from an overall point of view.

Finally, it should be mentioned that the probability density function (*PDF*) can be computed from the *CDF*, which can show the percentage of cells corresponding to different *PoF* values.

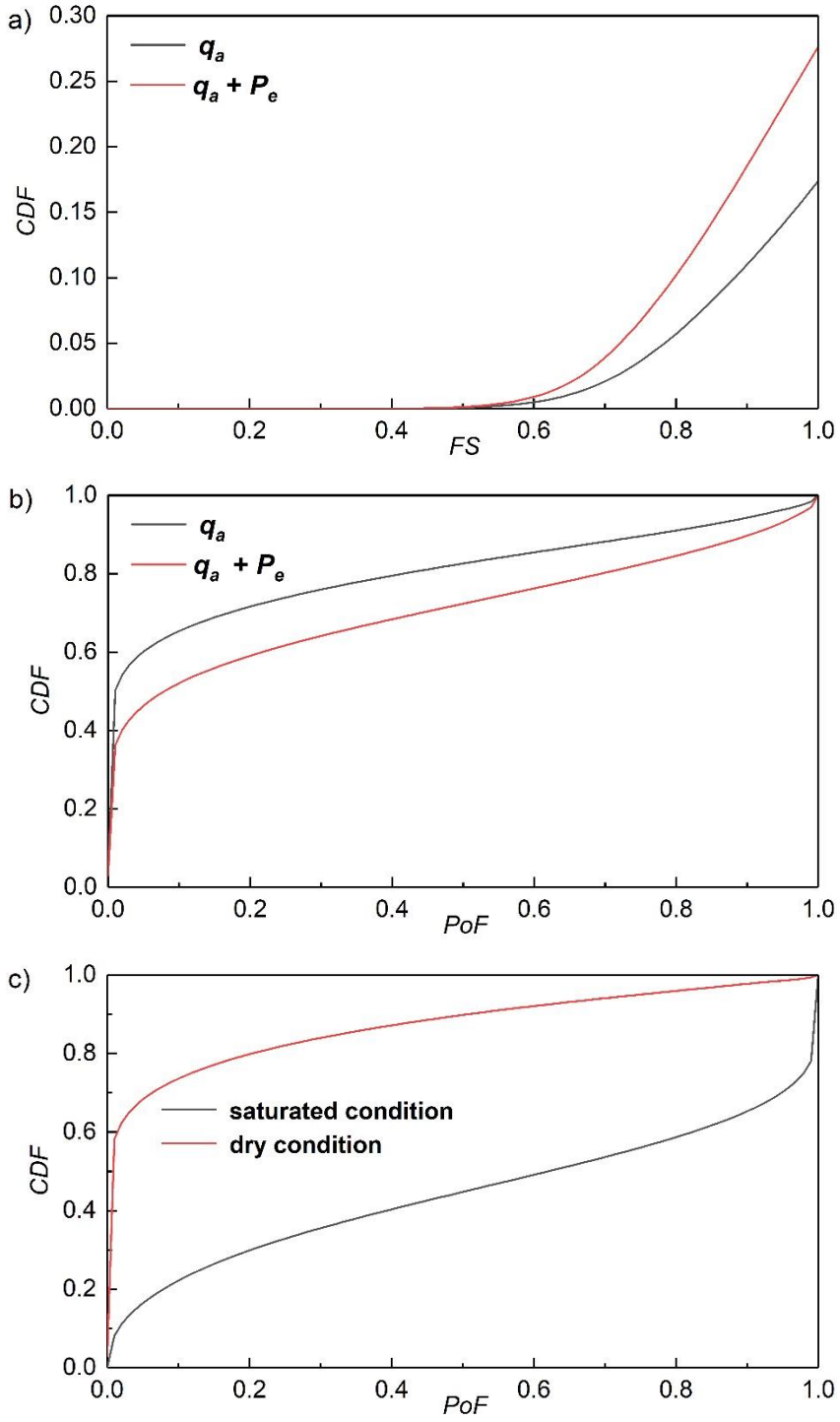

Figure 10 a) The cumulative distribution function (*CDF*) versus *FS* after q_a, and after q_a and P_e, respectively, b) The *CDF* versus *PoF* after q_a, and after q_a and P_e, respectively, and c) The *CDF* versus *PoF* under totally saturated and dry conditions, respectively.

3.2.3. Performance analysis and scientific interpretation

In this section, we switch to a supplementary external analysis of the plugin (see flowchart in Figure 1) using the existing landslide inventory and present the example of a performance analysis for

the landslide susceptibility map. Such a performance analysis is a standard part of landslide susceptibility assessment.

The percentage of points versus the *PoF* (Figure 11a) showed the evident negative effects of q_a and P_e on landslide points. Before applying rainfall, most of the landslide points had a *PoF* less than 0.2. After q_a and P_e , more than 45% points had a *PoF* larger than 0.8. On the contrary, the *PoF* change of the random points was very slight. Before the rainfall, 9% points had *PoF* larger than 0.8, and this ratio only increased by 10% after q_a and P_e.

The model accuracy was also clarified by the *ROC* analysis results (Figure 11b). The area under the curve was 0.69 when using the landslide points for analysis. After adding a buffer zone around the landslide points (due to the uncertainty on the landslide inventory points location), the *AUC* value improved evidently. When the buffer zone had a radius of 25 m, the *AUC* reached to 0.89 at its highest value, which was satisfactory. Considering that the landslide inventory of the 1982 episode has a rather low precision, applying a buffer is justified and the resulting accuracy is acceptable.

The results regarding the confusion matrix (Table 4) showed that by using the 0.1 as the *PoF* threshold, the *TPR* was 0.797 when no buffer zone is applied around the landslide points. The distance to the perfect classification was 0.647 in this condition. When the radius of the buffer zone increased, the *TPR* increased whereas the distance to the perfect classification decreased. Similarly, the accuracy increased from 0.647 (no buffer) to 0.737 (25-m buffer). All these indexes indicate that the landslide susceptibility map captures most of the landslide occurrences in the region and the result performance is good. However, it should be also noted that the *FPR* values didn't change in different conditions, so false positives should be also paid attention in the final application of the plugin, especially employing it for early warning systems.

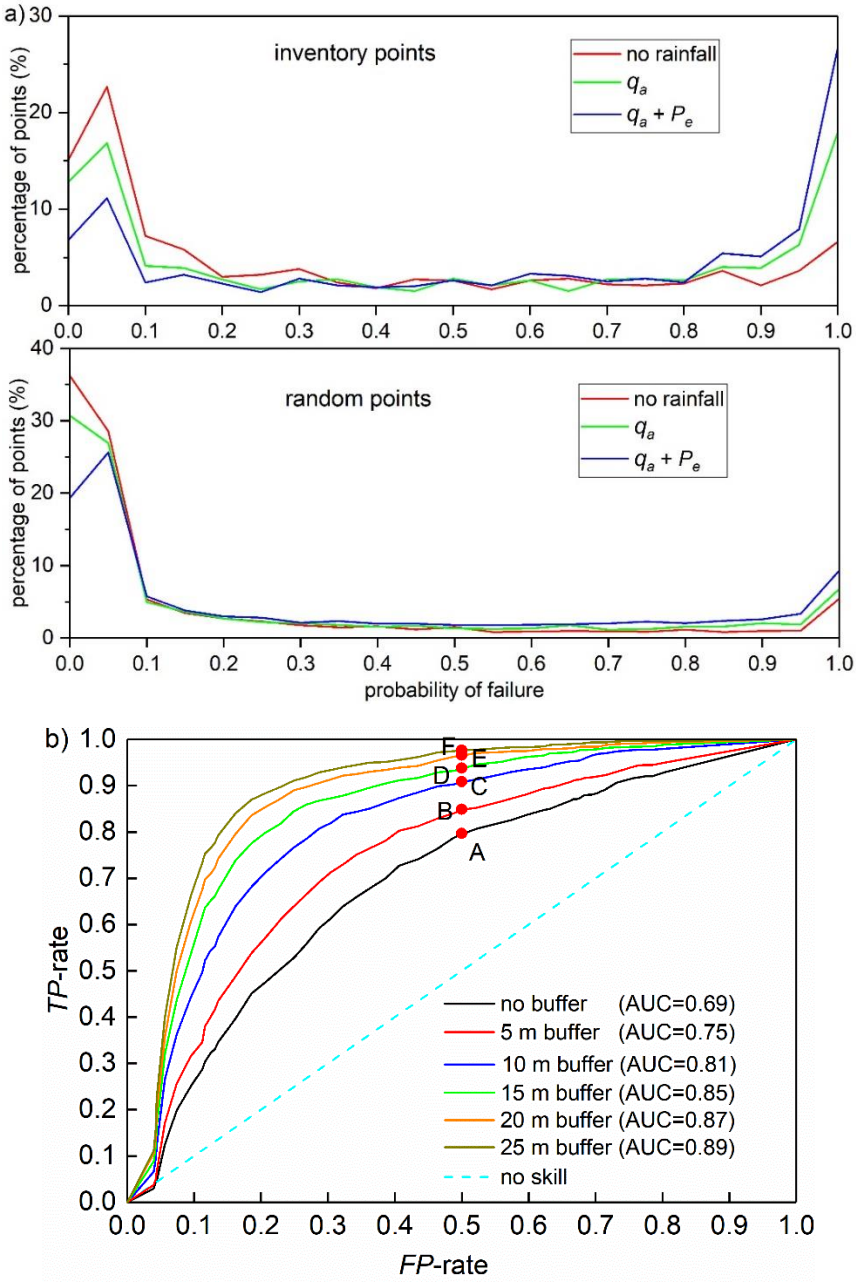

Figure 11 Evaluation of the stability modelling results for the 1982 rainfall episode in Berguedà area: (a) comparison between inventory points and random points under different rainfall conditions, (b) *ROC* curves and *AUC* values with/without buffer zone around inventory points. The red point in each curve shows the corresponding *FRR* and *TPR* values when *PoF*=0.1. The distances from these points to the perfect classification are shown in Table 4.

Table 4 The confusion matrix when using the *PoF*=0.1 as the threshold of safety level of slope stability

Radius of the buffer zone	*TP*	*TN*	*FP*	*FN*	*TPR*	*FPR*	*ACC*	Distance to perfect classification
0	795	2486	2514	203	0.797	0.503	0.647	0.647 (A)
5 m	847	2486	2514	151	0.849	0.503	0.673	0.673 (B)
10 m	907	2486	2514	92	0.909	0.503	0.703	0.703 (C)
15 m	936	2486	2514	64	0.938	0.503	0.718	0.718 (D)
20 m	964	2486	2514	34	0.966	0.503	0.732	0.732 (E)
25 m	975	2486	2514	23	0.977	0.503	0.737	0.737 (F)

4. Conclusions

In the present study, a Python QGIS plugin named FSLAM is introduced. It allows to compute regional shallow landslide susceptibility combining the effect of antecedent and event rainfall conditions, through GUI-based workflow in QGIS. An additional runoff module can also be used to obtain the peak discharge. The plugin outputs involve multiple data, including the raster maps regarding topography, rainfall infiltration, saturated degree of soil layer, factor of safety, and probability of failure, which can be selected individually by the users. The plugin was tested in the area of Berguedà, Spain, by analysing the landslide events triggered by 1982 rainfall episode. The results showed that the computational time for the area, containing in total 30 million pixels, only lasted 5 minutes. The accuracy of the landslide susceptibility map reached 89% when a 25 m- radius buffer was added around the landslide initiation points, indicating a satisfactory performance of the plugin.

The current version of the plugin has been released in GitHub repository, allowing automatic downloading and further extension and adaption. Future possible incorporation into the FSLAM plugin may focus on auto-calibration routines, and an additional module, which would directly show some results about the performance (e.g., comparison between the landslide inventory and random points, and the calculation of *ROC* scores).

5. Software availability

Name of Software: FSLAM.

Software version: 1.0.

Developers: Zizheng Guo; Vicente Medina

Software license: The GNU General Public License v3.0

Contact Address: Division of Geotechnical Engineering and Geosciences, Department of Civil and Environmental Engineering, BarcelonaTECH UPC, Jordi Girona 1-3 (D2), 08034 Barcelona, Spain.

Email: cuggzz@cug.edu.cn

Availability: https://github.com/EnGeoModels/fslam_plugin

Acknowledgements

This study was partly funded by the Spanish national projects SMuCPhy and EROSLOP (BIA 2015-67500-R and PID2019-104266RB-I00/AEI/10.13039/501100011033). Zizheng Guo acknowledges the financial support of China Scholarship Council for his research at UPC BarcelonaTECH, Fundamental Research Funds for National Universities, China University of Geosciences (Wuhan), and China Shaanxi Province key research program (No.2019ZDLSF07-07-02).

References

Althuwaynee, O.F., 2021. LaGriSU v 0.2 (Landslide Grid and Slope Units): binary (1,0) samples extraction tool pack for landslides mapping in QGIS. https//github.com/Althuwaynee/LaGriSU_Landslide-G. Last accessed 7 June, 2021.

AutoDeskInc, 2015. AutoCAD - overview. http//www.autodesk.com/products/autocad/overview#. Last accessed 23 March, 2021.

Baeza, C., 1994. Evaluación de las condiciones de rotura y de la movilidad de los deslizamientos superficiales mediante el uso de técnicas de análisis multivariante, Ph.D.-Thesis. Technical University of Catalonia, Barcelona. http://hdl.handle.net/2117/93582.

Bartolini, S., Cappello, A., Martí, J., Del Negro, C., 2013. QVAST: A new Quantum GIS plugin for estimating volcanic susceptibility. Nat. Hazards Earth Syst. Sci. 13, 3031–3042. https://doi.org/10.5194/nhess-13-3031-2013

Bathurst, J.C., Burton, A., Clarke, B.G., Gallart, F., 2006. Application of the SHETRAN basin-scale, landslide sediment yield model to the Llobregat basin, Spanish Pyrenees. Hydrol. Process. 20, 3119–3138. https://doi.org/10.1016/S0169-555X(99)00046-X

Baum, R.L., Godt, J.W., 2010. Early warning of rainfall-induced shallow landslides and debris flows in the USA. Landslides 7, 259–272. https://doi.org/10.1007/s10346-009-0177-0

Baum, R.L., Savage, W.Z., Godt, J.W., 2008. TRIGRS — A Fortran Program for Transient Rainfall Infiltration and Grid-Based Regional Slope-Stability Analysis, Version 2.0. U.S. Geol. Surv. Open-File Rep. https://doi.org/Open-File Report 2008–1159

Broeckx, J., Vanmaercke, M., Duchateau, R., Poesen, J., 2018. A data-based landslide susceptibility map of Africa. Earth-Science Rev. 185, 102–121. https://doi.org/10.1016/j.earscirev.2018.05.002

Chow, V.T., Maidment, D.R., Mays, L.W., 1988. Applied Hydrology, McGraw-Hill Series in Water Resources and Environmental Engineering. International Edition, McGraw-Hill Book Company, New York.

Clotet, N., Gallart, F., 1984. Inventari de degradacions de vessants originades pels aiguats de novembre de 1982, a les altes conques del Llobregat i Cardener. Servei Geològic de la Generalitat de Catalunya, Barcelona.

Corominas, J., Alonso, E., 1990. Geomorphological effects of extreme floods (November 1982) in the southern Pyrenees, in: Hydrology in Mountainous Regions. IAHS no. 194, Lausanne, pp. 295–302.

Corominas, J., Moya, J., 1999. Reconstructing recent landslide activity in relation to rainfall in the Llobregat River basin, Eastern Pyrenees, Spain. Geomorphology 30, 79–93. https://doi.org/10.1016/S0169-555X(99)00046-X

Corsini, A., Mulas, M., 2017. Use of ROC curves for early warning of landslide displacement rates in response to precipitation (Piagneto landslide, Northern Apennines, Italy). Landslides.

https://doi.org/10.1007/s10346-016-0781-8

Criollo, R., Velasco, V., Nardi, A., Manuel de Vries, L., Riera, C., Scheiber, L., Jurado, A., Brouyère, S., Pujades, E., Rossetto, R., Vázquez-Suñé, E., 2019. AkvaGIS: An open source tool for water quantity and quality management. Comput. Geosci. 127, 123–132. https://doi.org/10.1016/j.cageo.2018.10.012

ECORISQ, 2021. ECQRISQ [WWW Document]. URL https://www.ecorisq.org/docs/USCS_soilclasses.pdf Last accessed 11 May 2021

Ellsäßer, F., Röll, A., Stiegler, C., Hendrayanto, Hölscher, D., 2020. Introducing QWaterModel, a QGIS plugin for predicting evapotranspiration from land surface temperatures. Environ. Model. Softw. 130, 104739. https://doi.org/10.1016/j.envsoft.2020.104739

Fawcett, T., 2006. An introduction to ROC analysis. Pattern Recognit. Lett. 27, 861–874. https://doi.org/10.1016/j.patrec.2005.10.010

Fell, R., Corominas, J., Bonnard, C., Cascini, L., Leroi, E., Savage, W.Z., and on behalf of the JTC-1 Joint Technical Committee on Landslides and Engineered Slopes, 2008. Guidelines for landslide susceptibility, hazard and risk zoning for land use planning. Eng. Geol. 102, 99–111.

Froude, M.J., Petley, D.N., 2018. Global fatal landslide occurrence from 2004 to 2016. Nat. Hazards Earth Syst. Sci. 18, 2161–2181. https://doi.org/10.5194/nhess-18-2161-2018

GENCAT, 2008. Climatic maps of Catalonia 1961-1990. https://www.meteo.cat/climatologia/atles_climatic/ Last accessed 18 June 2021.

Geotechdata, 2021. Geotechdata [WWW Document]. URL https://www.geotechdata.info/parameter/ Last accessed 11 May 2021

Giorgi, F., Lionello, P., 2008. Climate change projections for the Mediterranean region. Glob. Planet. Change 63, 90–104. https://doi.org/10.1016/j.gloplacha.2007.09.005

Google Chrome, 2018. Get more done with the new Chrome. https//www.google.com/chrome/. Last accessed 23 march, 2021.

Guzzetti, F., Carrara, A., Cardinali, M., Reichenbach, P., 1999. Landslide hazard evaluation: a review of current techniques and their application in a multi-scale study, Central Italy. Geomorphology 31, 181–216. https://doi.org/10.1016/S0169-555X(99)00078-1

Guzzetti, F., Reichenbach, P., Cardinali, M., Galli, M., Ardizzone, F., 2005. Probabilistic landslide hazard assessment at the basin scale. Geomorphology 72, 272–299.

Hürlimann, M., Corominas, J., Moya, J., Copons, R., 2003. Debris-flow events in the Eastern Pyrenees. Preliminary study on initiation and propagation., in: Rickenmann, D., Chen, C. (Eds.), 3rd Int. Conf. on Debris-Flow Hazards Mitigation. Millpress, Davos, pp. 115–126.

Hürlimann, M., Lantada, N., Gonzalez, M., Pinyol, J., 2016. Susceptibility assessment of rainfall-triggered flows and slides in the Central-Eastern Pyrenees, in: Aversa, S., Cascini, L., Picarelli, L., Scavia, C. (Eds.), XII Int. Symposium on Landslides and Engineered Slopes. CRC Press, Naples, pp. 1129–1136.

ICGC, 2021. Catàleg d'esllavissades MORLE: any 1982 al Berguedà i any 2013 a la Vall d'Aran (POCTEFA - PYRMOVE).

ICGC, 2018. Land use and land cover map of Catalonia in 1987. https://territori.gencat.cat/ca/01_departament/12_cartografia_i_toponimia/bases_cartografiques/medi_ambient_i_sostenibilitat/usos-del-sol/ Last accessed 18 June 2021.

ICGC, 2016. Geological map 1:50000. https://www.icgc.cat/Administracio-i-empresa/Descarregues/Cartografia-geologica-i-geotematica/Cartografia-geologica/Mapa-geologic-comarcal-1-50.000 Last accessed 11 May 2021.

ICGC, 2013. Terrain Elevation Model of Catalonia 5 x 5 meters. https://www.icc.cat/appdownloads/ Last accessed 11 May 2021.

Iverson, R.M., 2000. Landslide triggering by rain infiltration. Water Resour. Res. 36, 1897–1910. https://doi.org/10.1029/2000WR900090

Lambe, T.W., Whitman, R. V, 1979. Soil mechanics. Wiley, New York.

Lee, J.H., Park, H.J., 2016. Assessment of shallow landslide susceptibility using the transient infiltration flow model and GIS-based probabilistic approach. Landslides. https://doi.org/10.1007/s10346-015-0646-6

Lehmann, P., Or, D., 2012. Hydromechanical triggering of landslides: From progressive local failures to mass release. Water Resour. Res. 48, W03535. https://doi.org/10.1029/2011WR010947

Medina, V., Hürlimann, M., Guo, Z., Lloret, A., Vaunat, J., 2021. Fast physically-based model for rainfall-induced landslide susceptibility assessment at regional scale. CATENA 201, 105213. https://doi.org/10.1016/j.catena.2021.105213

Merghadi, A., Yunus, A.P., Dou, J., Whiteley, J., ThaiPham, B., Bui, D.T., Avtar, R., Abderrahmane, B., 2020. Machine learning methods for landslide susceptibility studies: A comparative overview of algorithm performance. Earth-Science Rev. 207, 103225. https://doi.org/10.1016/j.earscirev.2020.103225

Mergili, M., Marchesini, I., Rossi, M., Guzzetti, F., Fellin, W., 2014. Spatially distributed three-dimensional slope stability modelling in a raster GIS. Geomorphology 206, 178–195. https://doi.org/10.1016/j.geomorph.2013.10.008

Millán, M., Estrela, M.J., Caselles, V., 1995. Torrential precipitations on the Spanish east coast: The role of the Mediterranean sea surface temperature. Atmos. Res. 36, 1–16. https://doi.org/10.1016/0169-8095(94)00048-I

Mishra, S., Singh, V., 2013. Soil Conservation Service Curve Number (SCS-CN) Methodology (Vol.42), Springer Science & Business Media.

Montalbán, F., Manzano, A., Correa, L., Cabot, J., Godé, L., 2013. Recomanacions tècniques per alsestudis d inundabilitat d àmbit local. Barcelona, Catalan Water Agency. (In Spanish).

Montgomery, D.R., Dietrich, W.E., 1994a. A physically based model for the topographic control on shallow landsliding. Water Resour. Res. 30, 1153–1171.

Montgomery, D.R., Dietrich, W.E., 1994b. Landscape dissection and drainage-area slope thresholds, in: LTD, J.W. (Ed.), Process Models and Theoretical Geomorphology. Chichester.

Nielsen, A., Bolding, K., Hu, F., Trolle, D., 2017. An open source QGIS-based workflow for model application and experimentation with aquatic ecosystems. Environ. Model. Softw. 95, 358–364. https://doi.org/10.1016/j.envsoft.2017.06.032

O'Callaghan, J.F., Mark, D.M., 1984. The extraction of drainage networks from digital elevation data. Comput. Vision, Graph. Image Process. 28, 323–344. https://doi.org/10.1016/S0734-189X(84)80011-0

Pack, R.T., Tarboton, D.G., Goodwin, C.N., 1998. The SINMAP approach to terrain stability

mapping. Eighth Int. Congr. Int. Assoc. Eng. Geol. Environ. Proceedings, Vols 1-5 1157–1165.
Park, H.J., Lee, J.H., Woo, I., 2013. Assessment of rainfall-induced shallow landslide susceptibility using a GIS-based probabilistic approach. Eng. Geol. https://doi.org/10.1016/j.enggeo.2013.04.011
QGIS Development Team, 2021. QGIS Geographic Information System. Open Source Geospatial Foundation Project. http//qgis.osgeo.org Last accessed 17 April 2021.
Reichenbach, P., Rossi, M., Malamud, B.D., Mihir, M., Guzzetti, F., 2018. A review of statistically-based landslide susceptibility models. Earth-Science Rev. 180, 60–91. https://doi.org/10.1016/j.earscirev.2018.03.001
Reid, M.E., Christian, S.B., Brien, D.L., 2000. Gravitational stability of three-dimensional stratovolcano edifices. J. Geophys. Res. 105, 6043–6056. https://doi.org/10.1029/1999JB900310
Rigon, R., Bertoldi, G., Over, T.M., 2006. GEOtop: A distributed hydrological model with coupled water and energy budgets. J. Hydrometeorol. 7, 371–388. https://doi.org/10.1175/JHM497.1
Rossi, G., Catani, F., Leoni, L., Segoni, S., Tofani, V., 2013. HIRESSS: A physically based slope stability simulator for HPC applications. Nat. Hazards Earth Syst. Sci. 13, 151–166. https://doi.org/10.5194/nhess-13-151-2013
Santacana, N., 2001. Análisis de la susceptibilidad del terreno a la formación de deslizamientos superficiales y grandes deslizamientos mediante el uso de sistemas de información geográfica. Aplicación a la cuenca alta del río Llobregat. PhD-thesis, UPC, Barcelona.
Sela, L., Salomons, E., Housh, M., 2019. Plugin prototyping for the EPANET software. Environ. Model. Softw. 119, 49–56. https://doi.org/10.1016/j.envsoft.2019.05.010
Shu, H., Hürlimann, M., Molowny-Horas, R., González, M., Pinyol, J., Abancó, C., Ma, J., 2019. Relation between land cover and landslide susceptibility in Val d'Aran, Pyrenees (Spain): Historical aspects, present situation and forward prediction. Sci. Total Environ. 693, 133557. https://doi.org/10.1016/j.scitotenv.2019.07.363
Silva, F., Lambe, T.W., Marr, W.A., 2008. Probability and Risk of Slope Failure. J. Geotech. Geoenvironmental Eng. https://doi.org/10.1061/(asce)1090-0241(2008)134:12(1691)

Simoni, S., Zanotti, F., Bertoldi, G., Rigon, R., 2008. Modelling the probability of occurrence of shallow landslides and channelized debris flows using GEOtop-FS. Hydrol. Process. 545, 532–545. https://doi.org/10.1002/hyp

Strauch, R., Istanbulluoglu, E., Riedel, J., 2019. A new approach to mapping landslide hazards: A probabilistic integration of empirical and physically based models in the North Cascades of Washington, USA. Nat. Hazards Earth Syst. Sci. 19, 2477–2495. https://doi.org/10.5194/nhess-19-2477-2019

Témez, J.R., 1991. Extended and improved rational method. Version of the highways administration of Spain., in: Proc. XXIV Congress. Madrid, Spain. Vol A., pp. 33-40.

Témez, J.R., 1978. Calculo hidrometeorologico de caudales máximos en pequeñas cuencas naturales. Dirección general de carreteras, Spain. 124pp, ISBN: 84-7433-040-8.(In Spanish).

Titti, G., Sarretta, A., 2020. CNR-IRPI-Padova/SZ: SZ plugin (Version v0.1). Zenodo http://doi.org/10.5281/zenodo.3843275.

Tofani, V., Bicocchi, G., Rossi, G., Segoni, S., D'Ambrosio, M., Casagli, N., Catani, F., 2017. Soil characterization for shallow landslides modeling: a case study in the Northern Apennines (Central Italy). Landslides 14, 755–770. https://doi.org/10.1007/s10346-017-0809-8

Trapero, L., Bech, J., Duffourg, F., Esteban, P., Lorente, J., 2013. Mesoscale numerical analysis of the historical November 1982 heavy precipitation event over Andorra (Eastern Pyrenees). Nat. Hazards Earth Syst. Sci. 13, 2969–2990. https://doi.org/10.5194/nhess-13-2969-2013

USDA, 2007. National Engineering Handbook: Part 630 - Chapter 7: Hydrologic Soil Groups. National Resources Conservation Service, National Resources Conservation Service.

USDA, 1986. Urban hydrology for small watersheds. Technical release 55.National Resources Conservation Service. National Resources Conservation Service.

Wang, H.J., Xiao, T., Li, X.Y., Zhang, L.L., Zhang, L.M., 2019. A novel physically-based model for updating landslide susceptibility. Eng. Geol. 251, 71–80. https://doi.org/10.1016/j.enggeo.2019.02.004

Woodward, D., Hawkins, R., Hjelmfelt, A., Van Mullem, J., Quan, Q., 2002. Curve number method: Origins, applications and limitations., in: US Geological Survey Advisory Committee on Water

Information–Second Federal Interagency Hydrologic Modeling Conference. July 28-August 1, Las Vegas, Nevada.

Yu, B., 1998. Theoretical Justification of SCS Method for Runoff Estimation. J. Irrig. Drain. Eng. 124, 306–310. https://doi.org/10.1061/(asce)0733-9437(1998)124:6(306)

Zêzere, J.L., Pereira, S., Melo, R., Oliveira, S.C., Garcia, R.A.C., 2017. Mapping landslide susceptibility using data-driven methods. Sci. Total Environ. 589, 250–267. https://doi.org/10.1016/j.scitotenv.2017.02.188